Saltwater intrusion in delta regions around the world

MSc Thesis

July 31, 2020

Jonas Götte

Department of Physical Geography

Utrecht University

Supervisors:

Dr. ir. Niko Wanders

Dr. Josefin Thorslund

Student registration number: 6419097

Contact: jonas.goette@students.uu.nl / jonas.goette@gmail.com

MSc Research GEO4-1520

ECTS: 37.5

Abstract

The intrusion of saline sea water is a common phenomenon in deltas and threatens freshwater supply and ecosystems. Saltwater intrusion is mainly reported for specific regions or estuaries but has not yet been assessed on a global level. Due to projected changes in river discharge and sea level, a modification of the distance saltwater can travel upwards a delta can also be expected. Hence, salinity levels may further rise where they are already high or become more relevant where saltwater intrusion is not yet a reported issue.

This thesis describes a first attempt of modelling saltwater intrusion on the global scale by applying an existing analytical model for saltwater intrusion. For this purpose, a global discharge dataset was combined with a new dataset containing information about delta location and properties. The results show that saltwater intrusion is not uniform around the globe, but that there are regions like South-East Asia which experience higher distances of saltwater intrusion. These identified hotspots are in good agreement with previous findings from field studies, demonstrating the viability of the model outputs as valuable reference points for further investigations. The model also suggests that sea level rise will have a bigger impact on the intrusion lengths than changes in discharge conditions.

The study also identifies that an analytical intrusion model in general, but especially on a global scale, comes with numerous limitations and requires improvements in the future. The availability of salinity records to be used for calibration and validation is here the major issue, along with accurate information about deltaic shape.

Keywords: saltwater intrusion, deltas, global hydrological modelling, water resources, climate change

Acknowledgement

I would like to thank Niko Wanders for his idea about this topic for an MSc thesis, the guidance on global modelling and the general supervision during this project. Thanks also to my second supervisor, Josefin Thorslund, for her input about salinity in freshwater systems and the given feedback during the writing of this thesis. Furthermore, I like to thank Jaap Nienhuis for his recommendations and provision of data about delta morphology and geometry on a global scale. Thank you all.

Contents

List of Figures

List of Tables

1 Introduction

Delta regions are economically and ecologically important environments. A large part of the world's population has settled in river deltas and they form a centre for agricultural production (Pont *et al.*, 2002; Ericson *et al.*, 2006; Syvitski & Saito, 2007). Estuaries and deltas mark the transition zone from river to sea and hence also the transition from freshwater to saline water (Savenije, 2012). Intrusion of saline sea water into rivers is a natural phenomenon in delta regions (Huu-Thoi & Gupta, 2001; Savenije, 2012). Tidal-flow transports saline sea water landwards, until fresh river discharge and tidal flow are in balance. This distance is called the saltwater intrusion length (Savenije, 1993).

Salinization of riverine water may constrain its usage for irrigation and human consumption (UNEP, 2016) and also bring negative ecological impacts, such as eutrophication of coastal wetlands and biodiversity reduction (Ardón *et al.*, 2013; Noe *et al.*, 2013; Cañedo-Argüelles *et al.*, 2016). Saltwater intrusion is already an issue in many regions worldwide (e.g. Kaushal *et al.* 2018; Rahman *et al.* 2019) and changes in saltwater concentration related to climate change have already been experienced. For example, earlier onset of low discharge periods in the Mekong Delta have been reported, causing salt water to reach about 10-20 km further upstream than before (Toan, 2014). In the Bay of Bengal, Bangladesh, reported intrusion lengths exceed 100 km (Allison *et al.*, 2003).

Deltas are also increasingly exposed to various drivers that may enhance salinization risks in the future. This includes both natural drivers, such as reductions in river flow due to climatic changes as well as anthropogenic drivers, like pollution from industry and agriculture (Haddeland *et al.*, 2014). Climate change is also projected to increase the frequency and extent of droughts, due to temperature increases and changes to precipitation regimes (Dai, 2011, 2013; Prudhomme *et al.*, 2014). More severe hydrological droughts are particularly expected in the Mediterranean, central Europe, south-east Asia, eastern U.S. and northern Brazil (Dai, 2013; Wanders & Van Lanen, 2015; van der Wiel *et al.*, 2019). As a result of droughts, lower river discharge could allow saline water to travel further upstream, which increase the intrusion length. Sea level rise is also expected to amplify this effect as increased pressure of the sea will push saltwater further inland. With regards to direct human drivers, increasing irrigation demands and water extraction rates will also put further pressure on regions which are already experiencing water scarcity and salinization issues (Haddeland *et al.*, 2014) since increased water abstraction decreases river discharge and hence reduces the pressure freshwater can hold against intruding tidal flow.

Estimations of saltwater intrusion under global change are therefore crucial for planning and managing freshwater resources. This includes consideration of changes in average climatological conditions, as well as hydrological extremes, such as droughts. So far, saltwater intrusion has mainly been assessed on a local level in regions where direct impacts had been reported (e.g. Zhang *et al.*, 2013; Cai *et al.*, 2014; Toan, 2014).. Assessment of saltwater intrusion at the global scale are currently lacking, due to the complexity of the intrusion process and the required data which is difficult to obtain globally. Global estimations are needed

since hydrological changes will impact salinity levels around the world and thereby affect economies and ecosystems. This includes further intruding salt water in regions were salinity levels are already problematic, but potentially also to deltas which have not yet been highly impacted.

Modelling offers the potential to estimate unknown quantities in regions both with and without limited observations and to make predictions for future scenarios with changing hydroclimatic conditions. Case studies which have used hydraulic models for saltwater intrusion modelling (Buschman *et al.*, 2010; Doan *et al.*, 2014; Toan, 2014; Nga *et al.*, 2020), are usually based on the Navier-Stokes equations (with some variations or simplification, e.g. MIKE11, DELFT3D). These approaches have two major drawbacks for global modelling: they are computationally extensive and require much observational data for calibration. Field campaigns, including boat surveys (Savenije, 2012) or a network of salinity measurement stations, are necessary to gain appropriate salinity profiles required for proper calibration and validation. Since the majority of estuaries is not – or only poorly – gauged (Savenije, 2015), detailed salinity records are usually not available. Hence, an alternative modelling approach is required to estimate saltwater intrusion on a global level.

Savenije (1993) has presented a predictive model which can be used without prior calibration and should theoretically also be applicable on a global scale. While previous prediction approaches were mainly based on laboratory experiments and assumed a constant river cross-section, this approach incorporates estuary geometry, a crucial parameter for the balance of river freshwater discharge and tidal salt water intrusion (Savenije, 2012). The model has since been revised and improved (Savenije, 2012; Gisen *et al.*, 2015), integrated in a GIS-environment (Aerts *et al.*, 2000) and shown to be applicable for multi-channel estuaries as well as being used in different case studies (Nguyen & Savenije, 2006; Zhang *et al.*, 2011; Cai *et al.*, 2015). However, later versions of the model also require more information about tidal dynamics and the specific physiographic conditions, which is difficult to obtain on a global level. Simultaneously, the authors widely recommend calibration for each individual river. Since data about salinity in estuaries is very limited, this study will make use of certain case studies as calibration and use further approximations on a global scale, based on the original saltwater intrusion model by Savenije (1993). The availability of global datasets of deltas and discharge has improved in the recent past and allows approximation of parameters required for the model and hence an estimation on a global scale.

The overall aim to this study is to perform a first global estimate of saltwater intrusion length in delta regions. This includes an assessment of the actual intrusion length, but also of the uncertainties associated with the applied saltwater intrusion model. More specifically, this study will (i) assess the predictive capacity of the saltwater intrusion model in reproducing historic conditions, (ii) evaluate its accuracy on a global scale and (iii) project the effect of climate change on saltwater intrusion.

2 Material & Methods

2.1 Saltwater intrusion model

Saltwater intrusion length can be expressed for different stages within a tidal cycle. Savenije (1993) used the intrusion length at high water slack L^{HWS}, which describes the maximum extent of the intrusion during a tidal period and is therefore well in line with the objective of this study. Intrusion length at high water slack is computed as:

$$L^{HWS} = a\ ln\ (\frac{1}{\beta} + 1) \tag{1}$$

where a is the cross-sectional conversion length and

$$\beta = \frac{Ka}{\alpha_0 A_0} \tag{2}$$

with A_0 as the cross-sectional area of the estuary mouth, here calculated as the product of estuary mouth width and depth, K as "Van der Burgh's coefficient" and α_0 as a parameter related to the dispersion at the river mouth. K is related to the shape of the salt-intrusion curve and is further described by Savenije (1993b) based on Van der Burgh (1972). It appears to have a specific value for individual estuaries (Savenije, 1986, 1989). The parameter α_0 is related to the dispersion at the river mouth. Both, K and α_0, are preferably obtained by calibrating the model against saltwater intrusion measurements for each estuary. To make the model applicable without having to calibrate for each estuary, Savenije (1993a) developed predictive equations for the two parameters. Those are based on 45 salt intrusion length measurements which were taken at 15 estuaries around the globe.

Hereby, he obtained an empirical formulation for Van der Burgh's coefficient as

$$K = 0.16 * 10^{-6} \frac{h_0^{0.69} g^{1.12} T^{2.24}}{H_0^{0.59} b^{1.10} B_0^{0.13}}\ (0 < K < 1) \tag{3}$$

where h_0 is the tidal average depth, g is the gravitational acceleration on earth, T is the tidal period, H_0 is the tidal range at spring tide, b is the width convergence length and B_0 is the estuary width at the mouth. The expression of K is based on its correlation to the four ratios:

$$I = \frac{h_0}{b} \qquad II = \frac{H_0}{h_0} \qquad III = \frac{h_0}{B_0} \qquad IV = \frac{T\sqrt{g h_0}}{H_0}. \tag{4-7}$$

The empirical assessment of α_0 lead to the formulation of:

$$\alpha_0 = 220 \frac{h_0}{a} \sqrt{\frac{E_0 T g h_0}{-Q_f A_0}} \tag{8}$$

where E_0 is the tidal excursion and Q_f is the freshwater discharge. An overview of all used parameters and their data source is given in Table 1. The unitless and not directly to a specific parameter related coefficient

in equations 3 and 8 are followingly referred to as f_K and f_a and later used for model re-calibration (here: $f_K = 0.16 * 10^{-6}$ and $f_a = 220$).

2.2 Data

2.2.1 Data sources

The introduced model requires different types of input variables, which can be divided into three parts: *Estuary Geometry, River Discharge,* and *Tidal parameters.*

Estuary Geometry

Nienhuis *et al.* (2018, 2020) provide a dataset comprising almost 11000 deltas worldwide. Deltas are given as point locations and include, but are not limited to, information about channel slope, average discharge and tidal amplitude. Their prediction of the widening of an estuary mainly depends on the ratio between tidal and river discharge. The estimations are evaluated as very good compared to the actual measurements of 72 global deltas (Nienhuis *et al.*, 2018). The dataset provides the base for further calculations of the variables actually required, which is discussed in more detail in Chapter 2.2.2.

The localisation of a delta is based on the HydroSheds dataset (Lehner *et al.*, 2008) with a 15 arc-sec resolution for latitudes below 60° and the 1-min ETOPO1 grid (Amante & Eakins, 2009) for higher latitudes. Deltas are further filtered according to basin size and position at a coast (Nienhuis *et al.*, 2020).

River Discharge Data

The used discharge data originates from the PCR-GLOBWB 2.0 model, which is a global water balance model developed at Utrecht University (Sutanudjaja *et al.*, 2018). The model calculates the water balance on grid-cells and includes modules for meteorological forcing, land surface, groundwater, surface water, irrigation and water use. For this study, discharge was acquired at a resolution of 5 arc-min.

Two discharge datasets are used here:

a) an estimation of global average discharge under current climatic conditions and
b) a projection of global average discharge for the years 2070-2099, where the PCR-GLOBWB model was forced by the IPSL General Circulation Model (e.g. Dufresne *et al.*, 2013) for RCP8.5 climate scenario.

Tidal parameters

The tidal parameters include E_0, T and H_0. The tidal excursion E_0 is preferably individually measured during an intrusion event. However, due to the costly and uncertain measurement it is often also modelled (Parsa & Shahidi, 2010; Savenije, 2012). Savenije (2012) suggests an estimation of 14 km for a global average of tidal excursion, which is used in this study. For the tidal period, a diurnal tide with a period of 44440 seconds is used for all deltas, in line with the diurnal tide period used by Savenije (1993). Instead of using the tidal range at spring tide for H_0, the average tidal range is used here, which is provided within the global delta set from Nienhuis *et al.* (2018, 2020) and is based on the TOPEX database (Egbert & Erofeeva, 2002).

2.2.2 Data processing

The introduced delta does not directly provide the required input parameters for the saltwater intrusion model. To obtain the required parameters, some assumptions and predictions have to be made which follow Nienhuis *et al.* (2018) and Nienhuis (2020). Included intermediate steps are:

$$upstream\ width = 10 * Qprist^{0.5} \tag{9}$$

$$upstream\ depth = 0.6 * Qprist^{0.3} \tag{10}$$

where *Qprist* is the naturally occurring discharge without human interference like dams. The estuarine length scale L and width at the estuary mouth B_0 can then be derived as:

$$L = \frac{upstream\ depth}{channel\ slope} \tag{11}$$

$$B_0 = k * TidalAmp * L * beta + upstream\ depth \tag{12}$$

where *beta* = 100 and k = 1.1*10^{-4}.

Estuary depth is defined as

$$d = \frac{B_0}{beta} \tag{13}$$

and is hence here always 1/100th of the estuary mouth width.

In the absence of more detailed information about delta shape, this study assumed cross-sectional convergence length and width convergence length to be the same and to equal the estuarine length scale L.

Table 1: Type, resolution, and data source of used variables

Variable	Type, resolution	Source
B_0, L	Point-location	derived after Nienhuis (2020) & Nienhuis *et al.* (2020)
H_0, h_0	Point-location	Nienhuis *et al. (*2020)
Q_f	Raster, 5 arc-min	Sutanudjaja *et al.* (2018)
E_0, T	Global Value	Savenije (2012)

Merging datasets

All data has been provided in a *netCDF* format. The point-locations are matched with respective raster-cells from the discharge data set. Due to apparent differences between delta location definition and land-masked used in the PCR-GLOBWB dataset, the delta coordinates do not always match up with the appropriate discharge raster cells. Therefore, all raster cells of the discharge dataset in a window of ±0.25° in longitude and latitude around the delta locations were compared to the naturally occurring discharge *Qprist* of the delta dataset. The cell with the smallest derivation was then linked to the specific delta. The cell with the same index was later used for the future discharge dataset.

2.3 Model calibration

The introduced model (eq. 3 & 8) had been calibrated against individual input data for estuary geometry by Savenije (1993). A comparison between the point-locations of the global delta set, and respective manual measurements of delta width based on satellite imagery and the width in Savenije (1993), has shown that the position of the delta mouth is different among studies (see ch. 4.2.3). Since there is no pattern in the offset between apparent delta-locations, the model had to be re-calibrated. Therefore, available geometry data from the global dataset was combined with discharge and intrusion length measurements from Savenije (1993). Intrusion length measurements were corrected in regard to the different delta locations. This included an estimation of the locations of the deltas given by Savenije (1993) since they are just described by an estuary name and a value for the mouth width but without an exact location. The distance between the estimated delta point and the location from Nienhuis *et al.*, (2020) was then used to correct the saltwater intrusion length measurements. The procedure is sketched in Figure 1. Some estuaries listed by Savenije (1993) could not be found, or not appropriately matched with the global delta locations and had to be excluded from the model calibration. The full dataset used for calibration can be found in the appendix (Tab. 3).

Re-calibration was performed using the *optim* algorithm (R Core Team, 2020). A minimum root-mean-square error (RMSE) between calculated and measured (and corrected) saltwater intrusions lengths was used as the goal function. The optimisation algorithm has difficulties with finding a global optimum and hence depends on the *first-guess* input parameters (see discussion, Ch. 4.2.1). Therefore, two calibration variants have been applied next to the original calibration: (i) a limited optimum calibration (*lim-opt*), using the coefficients of Savenije (1993) as *first-guess* input coefficients and (ii) a full-optimum calibration (*full-opt*), based on a Monte-Carlo simulation of different first-guess coefficients, with each coefficient attaining values of $10^x \; with \; x \in \{-6, -4, -2, 0, 2\}$ leading to 6^5 different combinations.

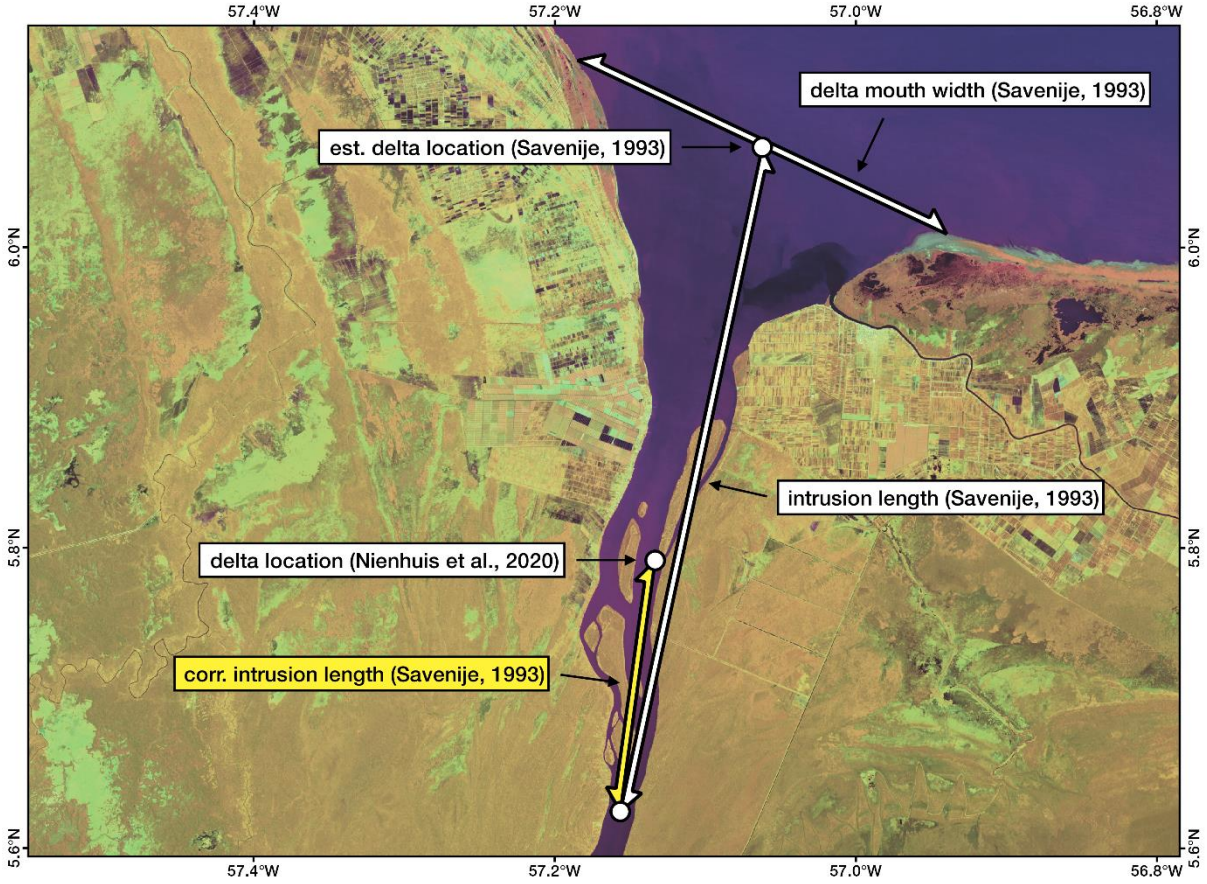

Figure 1: Estimation of the delta locations used in Savenije (1993) and correction of their intrusion length measurements based on the delta locations in Nienhuis *et al.* (2020)*; shown here exemplarily at the Corantijn river delta in South America. False-colour Landsat 5 image, dated 08/19/1992, courtesy of the U.S. Geological Survey.*

2.4 Implementation of sea level rise

A mean sea level rise of 0.5 m is used which is in line with the likely range of sea level rise projected for climate scenarios RCP4.5, RCP6.0 and RCP8.5 in years 2081 to 2100 relative to 1986-2005 (Church *et al.*, 2013). Sea level rise is here considered as uniform across the globe. While regional sea level rise can be quite variable, a more detailed representation of local effects is beyond the scope of this study.

Sea level rise leads to changing coastlines and increased sediment transport inlands and hence changes the position of delta outlets and their shape (e.g. Ranasinghe & Stive, 2009). Respective changes are currently not available in regard to the global delta dataset of Nienhuis *et al.* (2020) and can therefore not be considered. Consequently, the impacts of sea level rise had to be simplified and are implemented as a global uniform increase in delta mouth depth by 0.5 m.

3 Results

3.1 First global estimate of saltwater intrusion

This overview gives a first idea about the spatial distribution of saltwater intrusion around the globe. The following sections describe the improvement and re-calibration of the model and analyse its sensitivity to the input parameters. Subsequently, global saltwater intrusion will be projected using the improved model, which is then also used to show expected intrusion between 2070 and 2100 with an emphasis on estimated changes in comparison to current conditions.

A first estimate of saltwater intrusion on a global scale has been made by applying the model as supplied by Savenije (1993) with average discharge conditions. The map (Fig. 2) shows that most deltas of the world are expected to have a low saltwater intrusion, here classified as 96 % of all deltas having a calculated intrusion length below 10 km. However, higher intrusion lengths do also occur, and can be especially found in larger rivers. For example, the Amazon, the Brahmaputra, Mekong or St-Lawrence River all show more than 50 km of expected intrusion length. Other regions having multiple deltas with high intrusion lengths are parts of Western Europe, Western Africa, the North-West US, Alaska and North-East Russia. Particularly low intrusion lengths can be found along Central America, Japan, the Mediterranean, New Zealand and South Africa. While only a few deltas stand out with a high intrusion length in otherwise only slightly influenced by salter intrusion, as e.g. in South-East Africa or Northern Australia, high saltwater intrusion can in most cases most be clustered in the mentioned regions above.

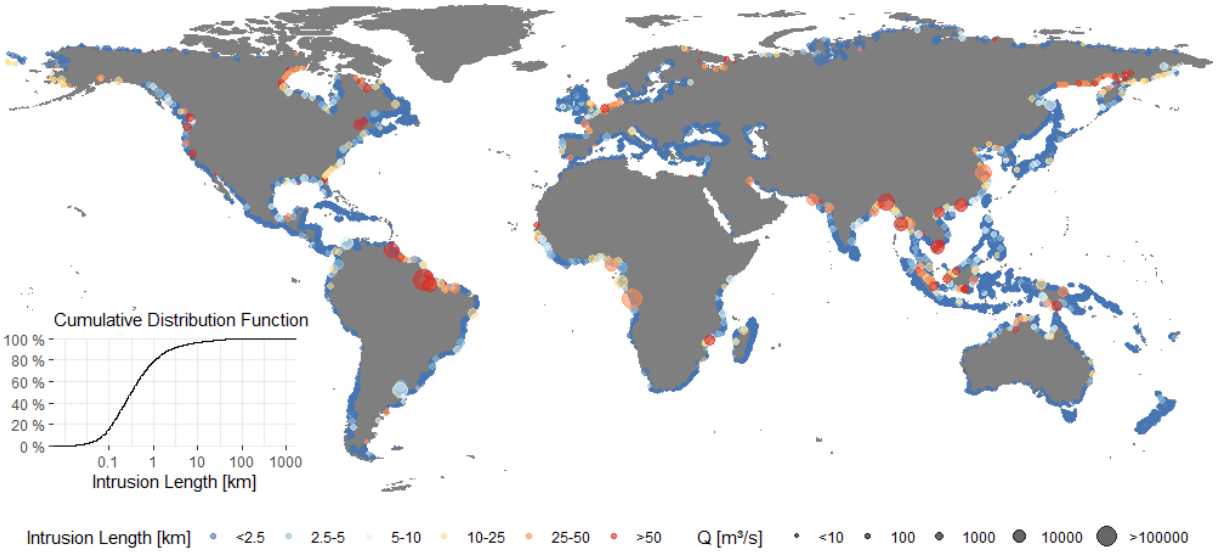

Figure 2: First estimate of saltwater intrusion for deltas around the globe, using the initial model from Savenije (1993).

3.2 Re-calibration and sensitivity

Differences between delta locations of the used datasets had to be considered for re-calibration of the model. The seven deltas targeted here had a mean distance of 16 km between delta location given by Nienhuis (2018) and estimated location derived from Savenije (1993), with a range of -1 km to 33 km with the delta position of the global dataset being further inland. The saltwater intrusion length measurements by Savenije (1993) were respectively corrected for these differences. The full input dataset for the calibration is depicted in the appendix (Tab. 3).

Re-calibration lead to quite different results for the set of coefficients for equations 4-7. The optimization result highly depends on the *first-guess* coefficients which must be supplied to the optimization algorithm. In the following, three calibration scenarios are used: a) the original calibration coefficients (Savenije, 1993), b) optimized coefficients using the original coefficients as *first-guess* input during the optimisation and c) optimized coefficients obtained from the described Monte-Carlo simulation using different inputs as *first-guess*.

Table 2 shows the obtained values for each of the six coefficients. Calibrations *original* and *lim-optim* are overall very similar, while *full-optim* deviates immensely from them. From the original calibration to *lim-optim*, α becomes more important in contrast to *K*, indicated by an increase in f_a and a decrease in f_K. For the calculation of *K* itself, the exponents for I and II decrease, while they increase for III, which implies a less importance of the estuary length, but higher sensitivity for the mouth width. While the fit between measured and modelled salt intrusion has decreased in terms of R^2 (0.051 to 0.041) the RMSE has also been reduced as aimed for in the goal function (29.17 to 23.2). Calibration *full-optim* lead to more promising results considering the statistical fit. The RMSE could be reduced to 10.64, while R^2 is here also much higher reaching 0.51. Exponents for I to IV are negative in this variant, which implies in combination with the highly risen f_K, a decreased relevance of the individual components in *K*, but a higher *K* in regard to alpha.

It needs to be pointed out, that this applied to the calculation of *K* only and does not consider respective changes of *a* which are part of the subsequent sensitivity analysis.

The resulting intrusion length values for the different calibrations are shown in Figure 3. The *original* calibration generally shows an underestimation of intrusion lengths for most cases, which slightly improves for *lim-optim* that moves intrusion lengths upwards. The *full-optim* calibration leads to values closer to the measurements, however, the calculation results are also more uniform and show less variation. This supports the previously introduced idea of an increased but more uniform intrusion length output and an overall lowered relevance of the actual inputs.

Table 2: Calibration results, including coefficients and statistical fit. The values shown here as I-IV represent the exponents of these components in the equation.

Calibration	I	II	III	IV	f_K	f_α	R^2	RMSE
original	1.1	1.66	0.13	2.24	$0.16*10^{-6}$	220	0.051	29.17
lim-optim	0.76	1.17	0.27	2.28	$2.44*10^{-9}$	243	0.041	23.20
full-optim	-0.51	-4.64	-6.95	-3.98	14.0	13.6	0.510	10.64

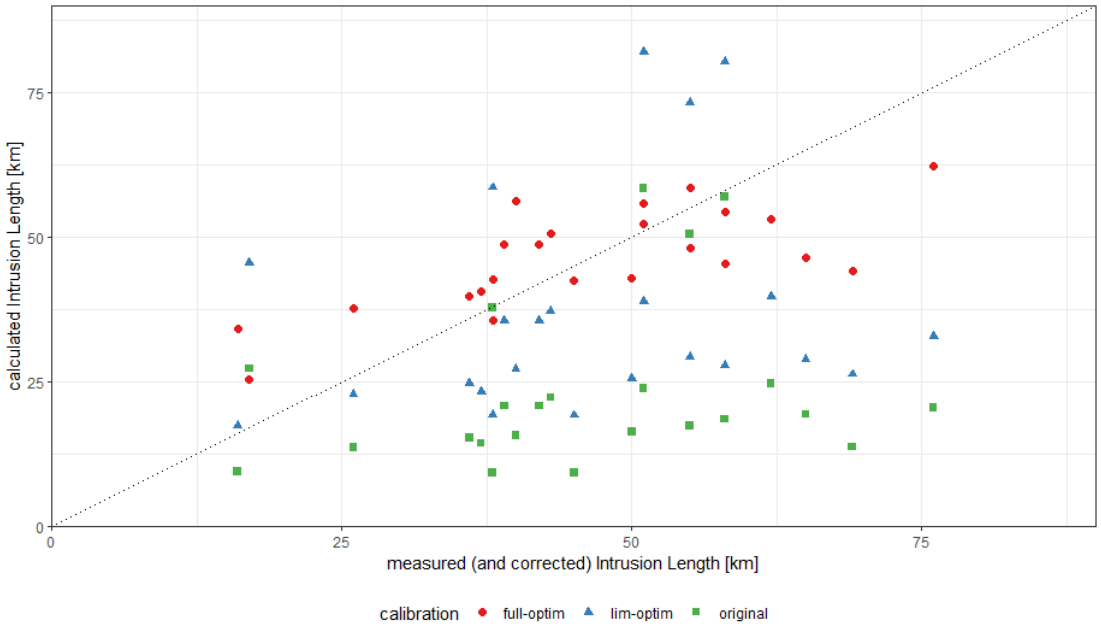

Figure 3: Saltwater intrusion length calculations for the sample cases of all three calibration scenarios

The obtained *K* values differ greatly between all three calibrations (Fig. 4). At this point it needs to be mentioned again, that the model is only applicable when $0 < K \leq 1$ applies (eq. 3, Savenije (1993)). The *original* calibration leads to too high cases, with *K* only falling for one delta in the appropriate range. *Lim-optim* and *full-optim* have all valid values for *K*. However, the *K* values resulting from c have maximum of 0.063, which is very low compared to Savenije's values and related to the high scaling factor for f_K applied afterwards. None of the new *K* values seems to fit well with the calibrated values from Savenije (x-axis), but due to strong differences in delta geometry between the datasets, a good fit cannot be expected (see Ch. 4.2.1).

Applying the three calibration on the entire global dataset, shows that the magnitude of calculated saltwater intrusion differs among them (Fig. 5). As already suggested by the calculation for the previous cases (Fig. 3), mean saltwater intrusion length increases form the *original* calibration to *lim-optim* and is even higher for

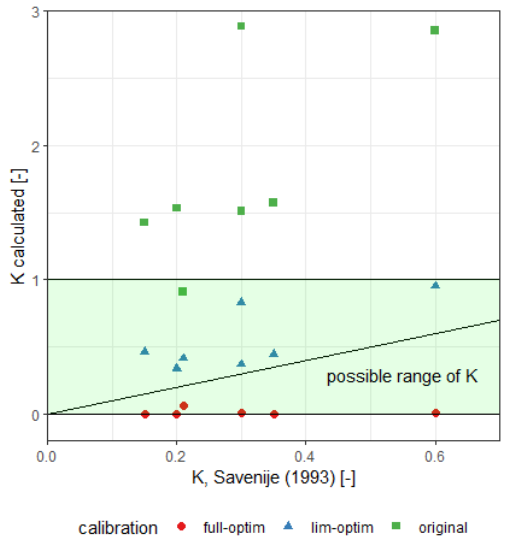

full-optim. While *original* expects 96 % of all deltas to have an intrusion length below 10 km, this percentage decreases to 92 % for *lim-optim* and 70 % for *full-optim*. Calibration *full-optim* has hence more than 30% of intrusion lengths above 10 km, with also more intrusion lengths above 100 km than the other calibrations.

Figure 4: Comparison of K between Savenije (1993) and calculations for the sample cases for all three calibration scnearios

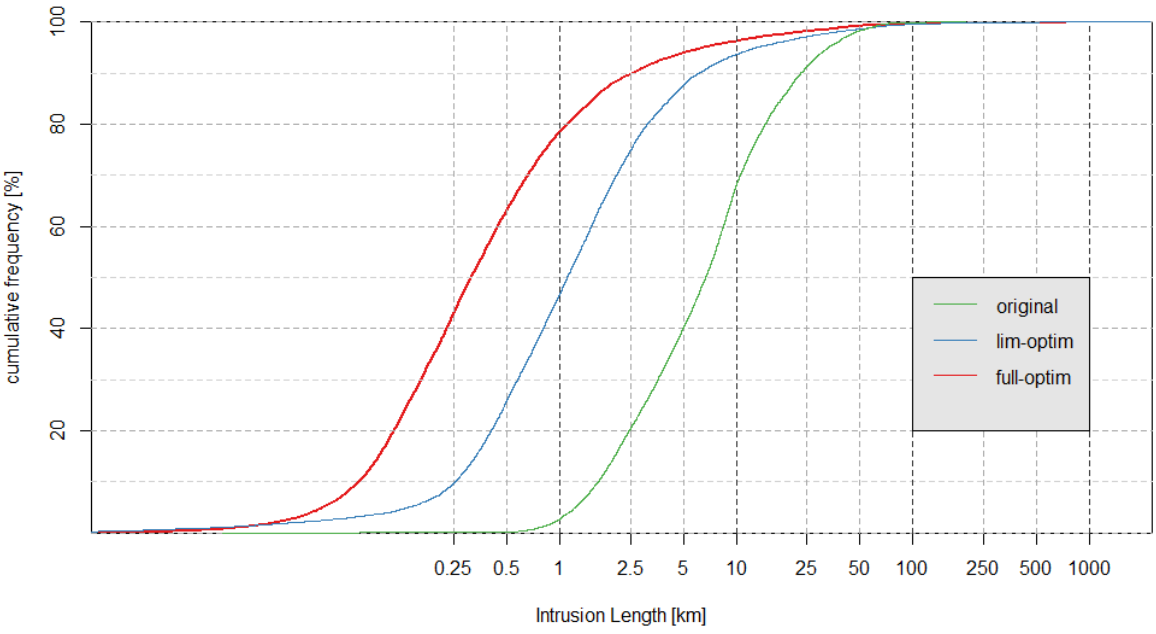

Figure 5: Cumulative frequency distribution of intrusion lengths for all deltas in different calibration scenarios

A global sensitivity analysis for the three different calibration settings shows similar results for the original and adapted coefficients but is different for the optimal calibration in the here applied range of ±20 % around the original values. All variants show an expected decrease of intrusion length with increasing discharge and an increase of intrusion length with decreasing length, tidal amplitude, and delta mouth width.

An increase in discharge of 20 % leads to a decrease of 6.3 ±1.3 % in intrusion length for the original parameter set and respectively 4 ±1.1 % and 1.1 ±1.1 % for calibrations *lim-optim* and *full-optim*. These are also most sensitive to changes in the delta mouth width. An increase of 20 % leads here to 27.8 ±7.1 %

increase in intrusion length and respectively 14.8 ±8.1 %. However, *full-optim* is insensitive to changes in the width, with just 0.82 ±0.86 % intrusion length increase for a 20 % increase in width.

Full-optim is most sensitive to the delta length with 13.3% ±6.2 % increase of intrusion length by 20 % increase in length. Overall, this scenario with the best fit shows very little sensitivity to all parameters except for the length. *Lim-optim and full-optim* are similar, with less than 0.5 % change of intrusion length per 1 % change in the input data for length, tidal amplitude and freshwater discharge. Only the sensitivity to the width is somewhat higher.

The previous analysis assesses the sensitivity considering the availability of the here used data on a global scale. This implies, that depth is not an independent input, but depends entirely on the delta mouth width. Usually, and as intended by Savenije (1993), these are independent measurements. Thus, the sensitivity for width and depth is followingly also shown independently.

The intrusion length appears to change in similar ways with increasing depth and width (slightly more for depth) for calibration *original* and *lim-optim* but differs for *full-optim* (Fig. 7). The calibration results suggest that the intrusion length actually increases with an increasing depth and decreasing width. This opposed response to the variable change balances each other out, when depth is dependent on width and ultimately leads to a near insensitivity of intrusion length to width in the previous analysis (Fig. 6).

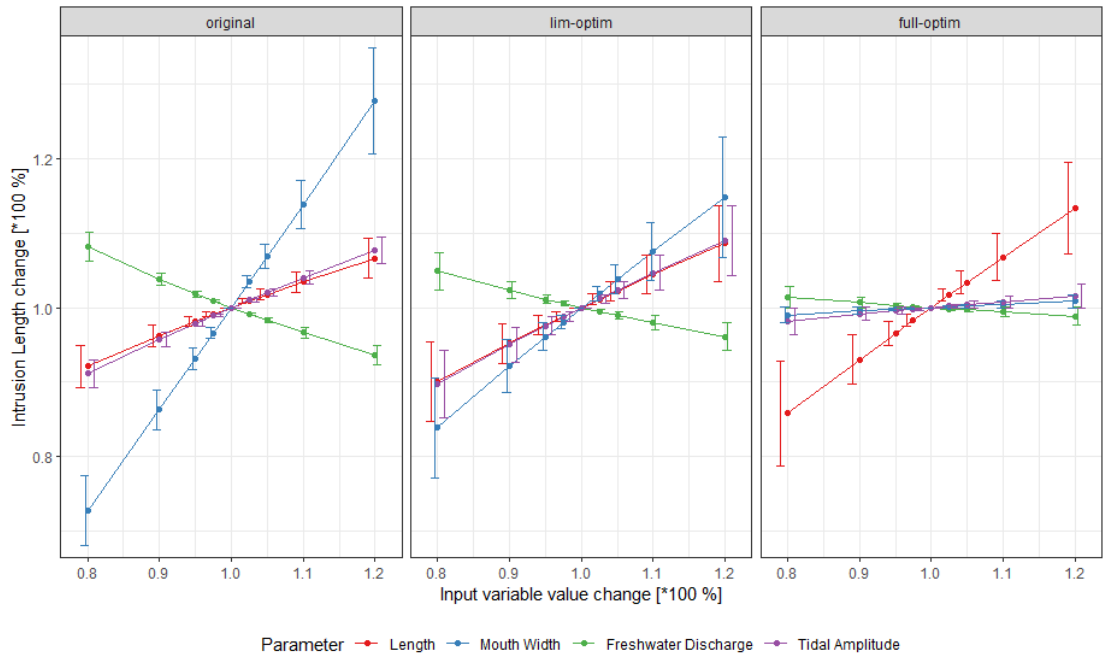

Figure 6: Results for the global sensitivity analysis for each calibration. Each variable was changed individually (x-axis) with the effect on intrusion length being calculated for all deltas on the globe. The results are here depicted with their mean and standard deviation of relative intrusion length change (y-axis). The change of mouth width includes a respective change of depth (eq. 13).

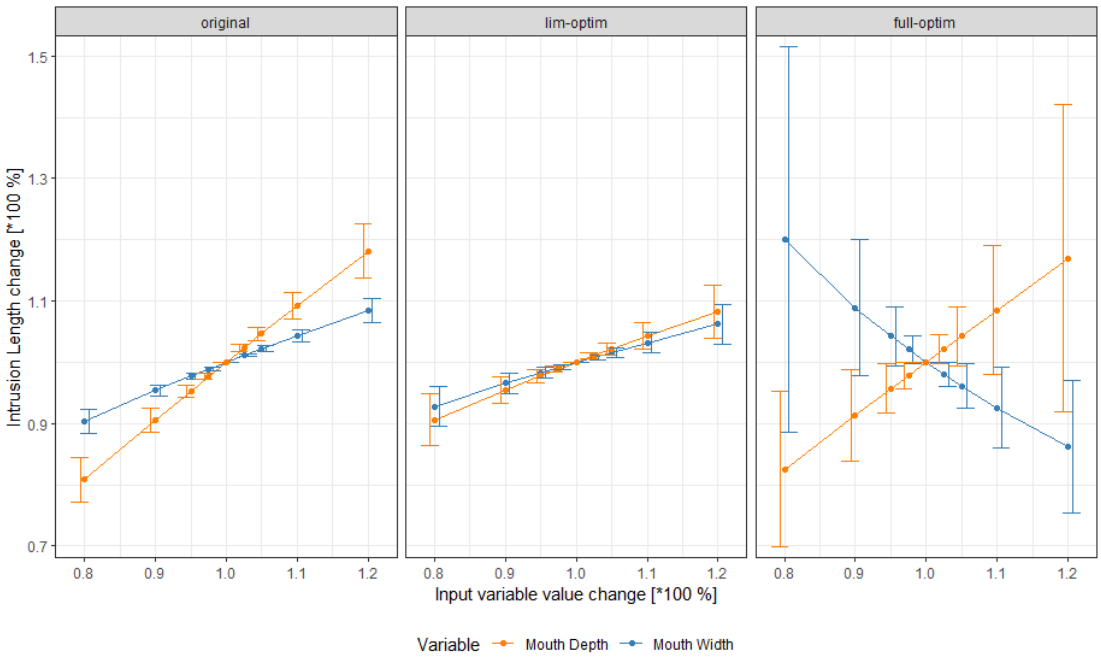

Figure 7: Results for the sensitivity analysis with a separate consideration of width and depth.

Overall, it can be concluded from the re-calibration, that the model outcome highly depends on its calibration. In this case, *lim-optim* appears as an improved version of the original calibration, leading to realistic values for *K* and a parameter sensitivity on the same scale to the original calibration. The *full-optim* calibration provides a good statistical fit to the data. However, the analysis of *K* and sensitivity have shown some clear deviation from the original calibration, including a reversed response to the width parameter and acceptable, but very low *K*-values. Hence, calibration *lim-optim* has been chosen for further assessment of intrusion length on a global scale with further implications of the calibration results being discussed later.

3.3 Current global intrusion

The global overview of estimated intrusion length is shown in Figure 8 and is comparable to the initial intrusion map presented in Chapter 3.1. As previously indicated, most deltas on the globe are estimated by the model to have an intrusion length below 10 km. Higher intrusion lengths are calculated for some deltas spread over the globe, but focus on South-East Asia, the North Sea coast, the Amazon region and some coastal regions in high latitudes around the Hudson Bay (Canada) or the Sea of Okhotsk (North-East Russia). Moderate intrusion lengths (10-25 km) can also be found in Western Africa or the North American West coast.

Core regions of higher intrusion lengths are South-East Asia, the Amazon region and the European North Sea coast. Additionally, mainland coasts in high latitudes (Eastern Russia, Hudson Bay) also have high intrusion lengths above 25 km.

Generally, large rivers appear to have high intrusion lengths, exemplarily the Amazon, Brahmaputra, Congo, Mekong, Yangtze or the Rhine. Here, modelled Intrusion lengths can rise over 500 km for the widest or longest deltas (Fig. 9). While there is a visible tendency for higher intrusion lengths with longer and wider deltas, the relationship is less clear for the tidal amplitude and only weak for discharge.

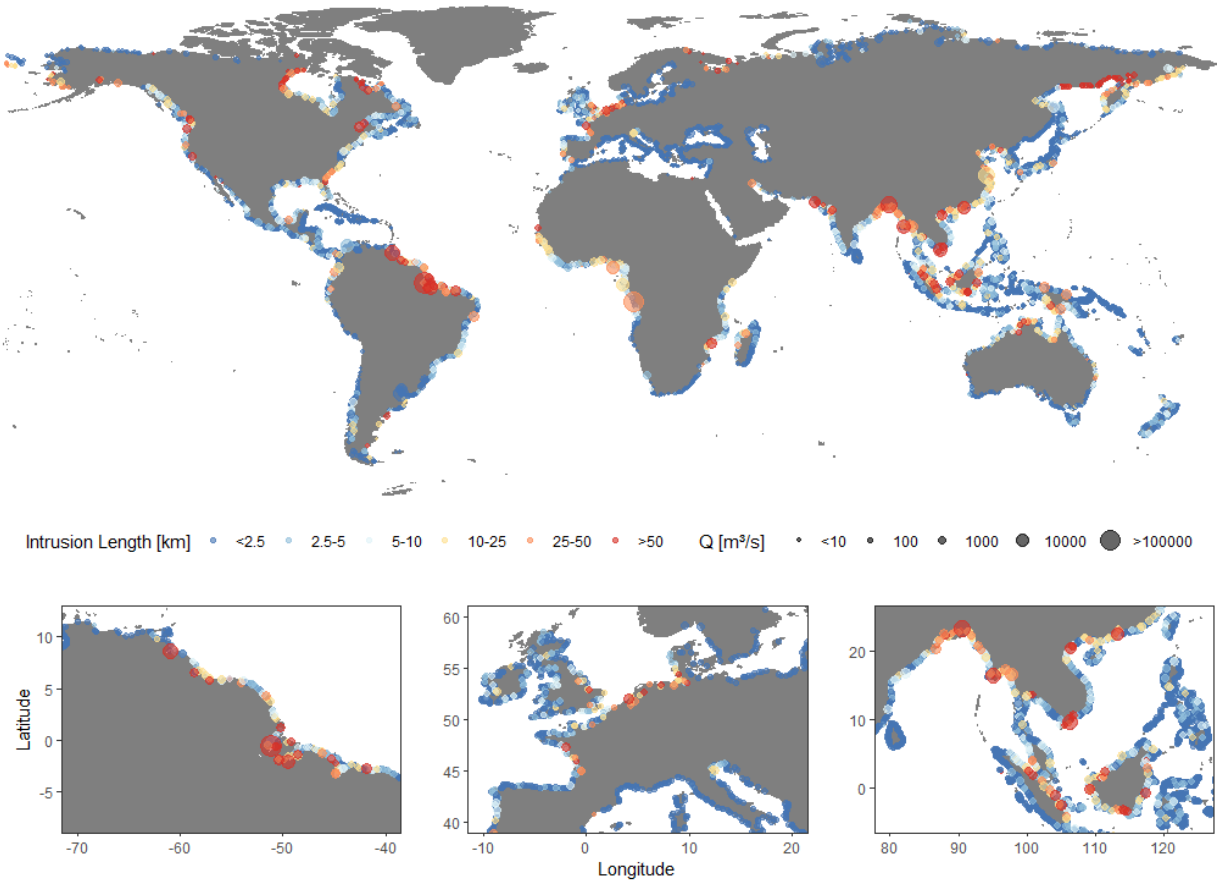

Figure 8: Modelled Intrusion Length around the globe based on the lim-optim calibration. Zoomed plots include regions with deltas with high intrusion lengths and are: NW South America, Central Europe and SE Asia (left to right).

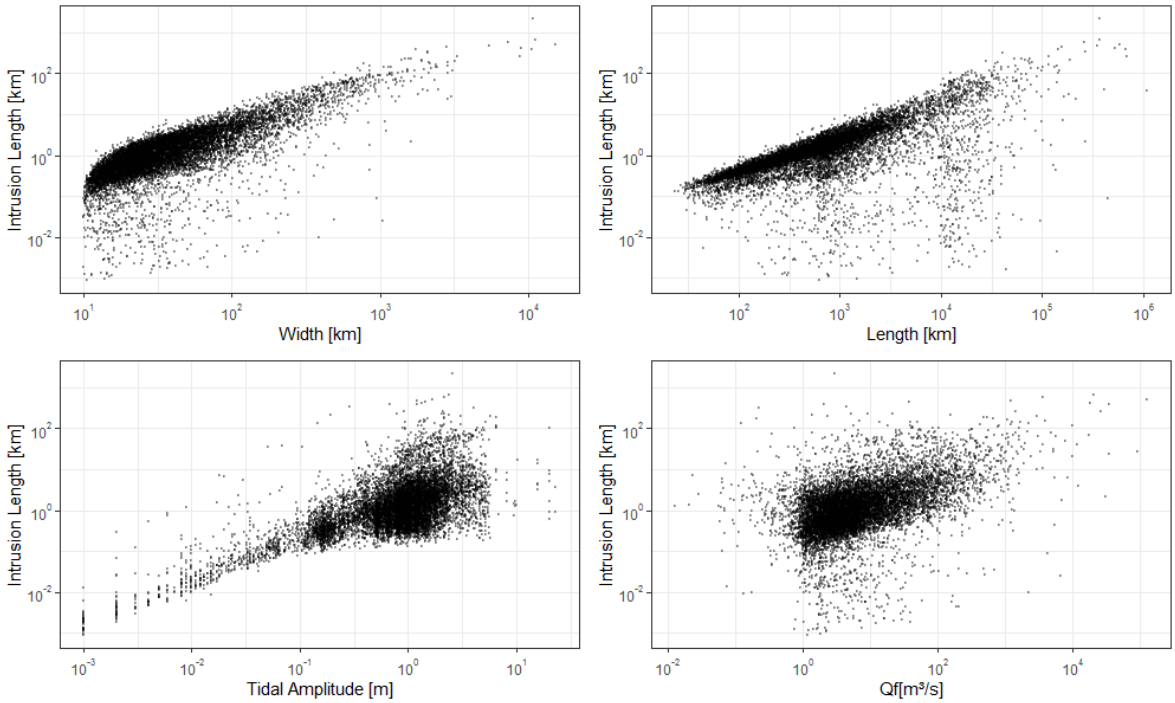

Figure 9: Scatter plots for the relationships between intrusion length and different input parameters.

3.4 Future scenario

3.4.1 Discharge change

Projections of a future scenario were also made using the *lim-optim* calibration. Figures 10 and 11 show the expected relative changes in intrusion length, based on discharge changes from current conditions to the projected average between 2070 and 2099.

Looking at the global overview of change, some patterns can be highlighted. In most of the tropics an increase in intrusion length is estimated. The west coast of Central and South America, as well as some deltas in Western Africa and South-East Asia show high levels of increase in intrusion. Additionally, the Eastern US Coast, Chinese East Coast and Northern Alaska also show an expected increase in intrusion length. In contrast, almost all deltas above 40° N expect a mostly consistent or decreasing intrusion length. The highest relative decreases can be observed in Northern Russia and Scandinavia. Some sub-tropical regions as the Indian Peninsula or Indonesia also expect less intrusion.

The change in intrusion length in South-East Asia is quite variable. The large rivers Brahmaputra and Mekong do not appear to experience much change in intrusion length, based on change in average discharge. However, many smaller rivers show a decrease in discharge and respectively their intrusion length. The island of Borneo stands out with expected decrease in intrusion length of over 50 % on its

south and west coasts, the intrusion length in the deltas on the east coast remain largely constant and, in some cases, increases.

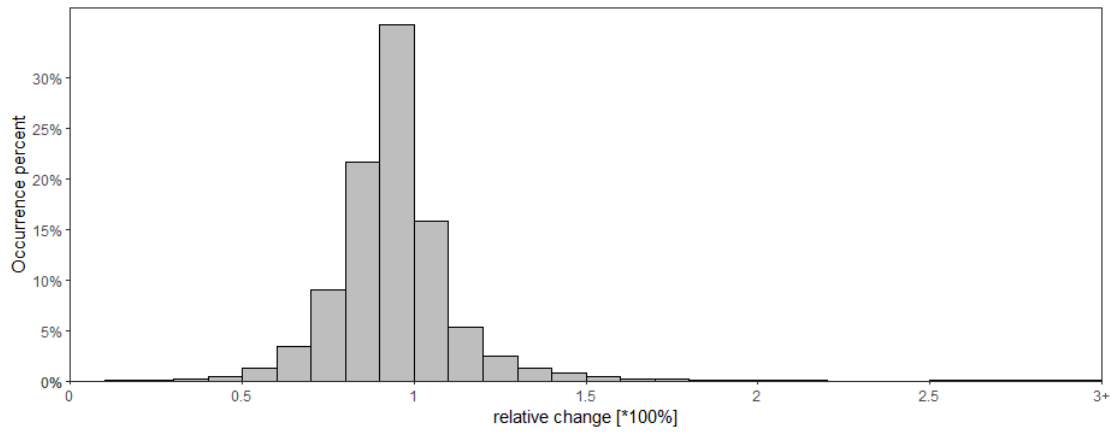

Figure 10: Histogram of global relative changes in intrusion length, with the various change factors shown on the horizontal axis and their occurrence percentage on the vertical axis.

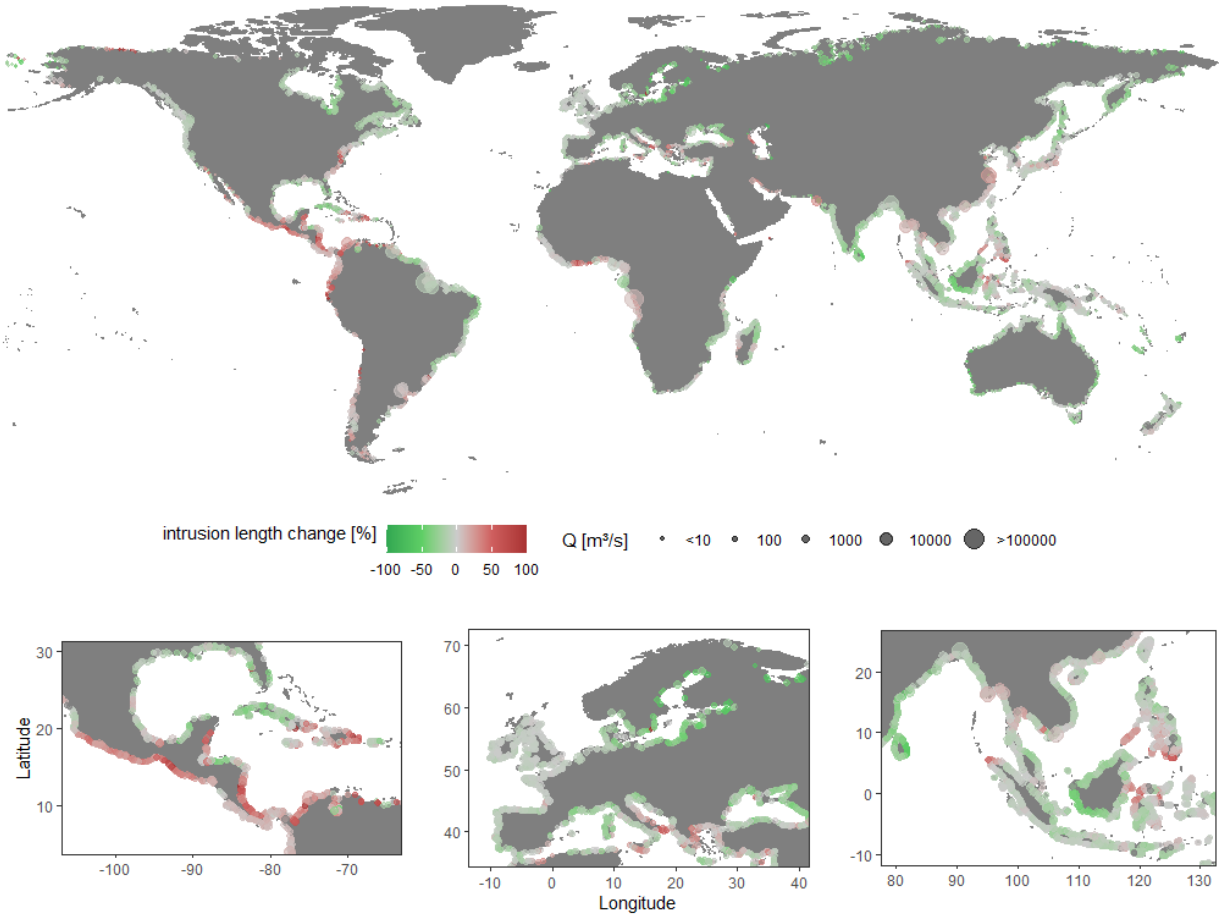

Figure 11: Projected global changes in intrusion length between current conditions and the average of 2070 to 2099.

Considering all deltas on the globe, the vast majority (75 %) can expect a decline in intrusion length which is around 0 to 20 % for 55 percent of all deltas. Only 5 % of all deltas can expect an increase in intrusion length above 20 %.

The relative changes are supposedly quite reliable since the different calibration methods have shown to lead to a similar scale of sensitivity to discharge for all calibrations, even if the absolute results for the intrusion length may be quite different. However, to identify the hotspots of saltwater intrusion, it is still required to consider at the absolute values (Fig. 12). Exemplarily, a region with a high relative change like Central America, usually still shows projected intrusion lengths below 10 km in the future. The previously identified regions and deltas with a high intrusion length (e.g. Mekong, Amazon or North Sea) are not expected to have major changes in intrusion lengths due to changes in discharge but are still hotspots of saltwater intrusion in absolute terms in the future.

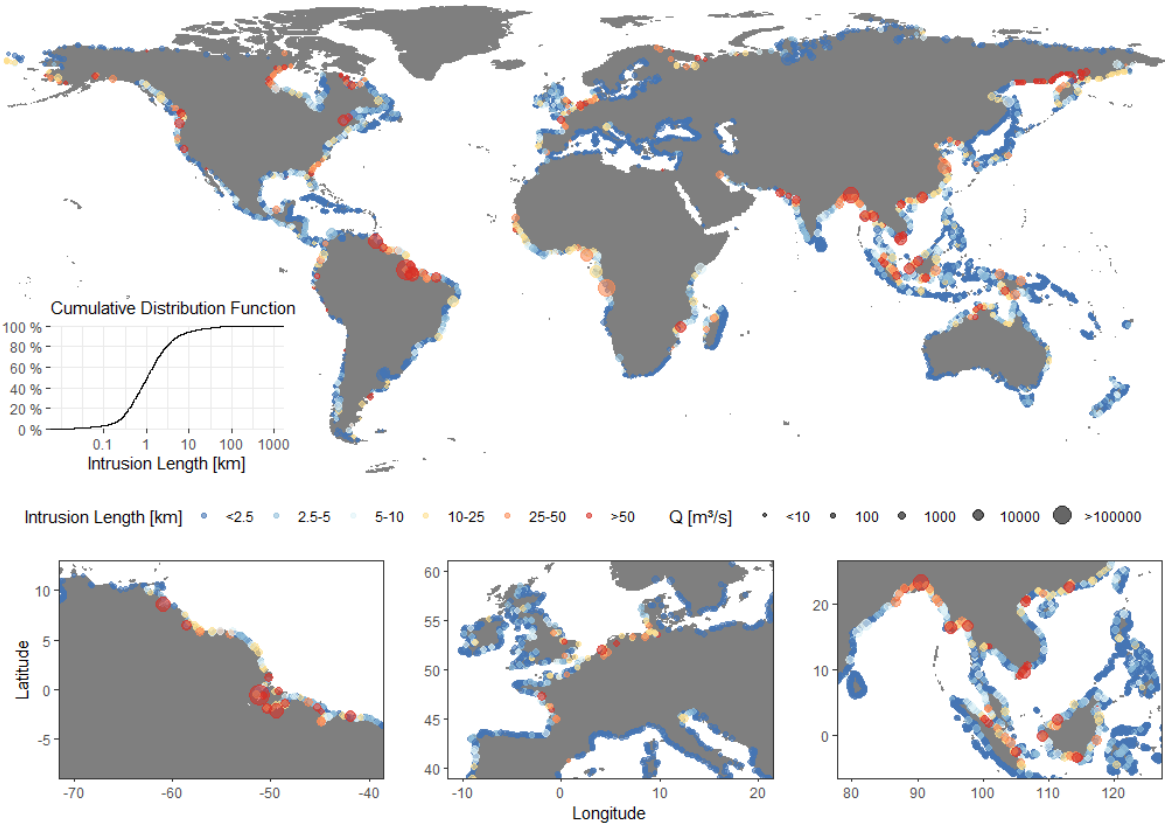

Figure 12: Estimated average saltwater intrusion between 2070 and 2099.

3.4.2 Sea level rise

An assumed global sea level rise of 0.5 m leads to increased saltwater intrusion around the globe. This originates from the model, where an increase in depth leads to an increase in saltwater intrusion (Ch. 3.2, Fig. 7). Overall, 75 % of all deltas can expect an increased intrusion length up to a factor of 1.5 as a result of the assumed sea level rise (Fig. 13). The magnitude of change is related to the original depth of the estuaries. If the original depth is low, the relative change in depth is high which usually leads to a higher change in intrusion length (Fig. 14).

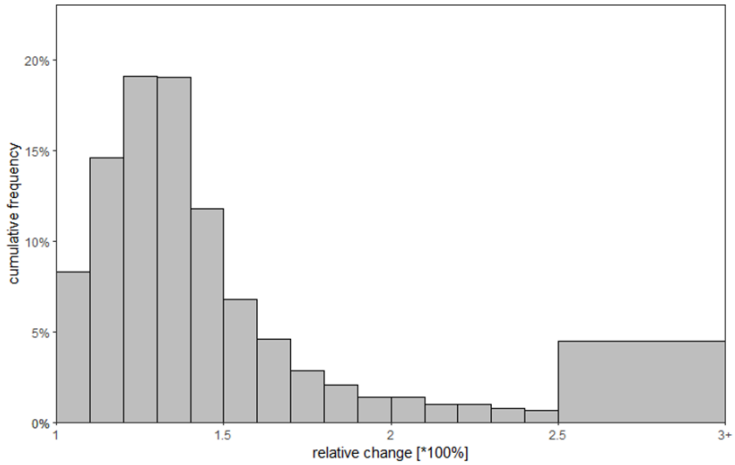

Figure 13: Histogram of global relative changes in intrusion length in regard to a sea level rise of 0.5 m, with the various change factors shown on the horizontal axis and their occurrence percentage on the vertical axis.

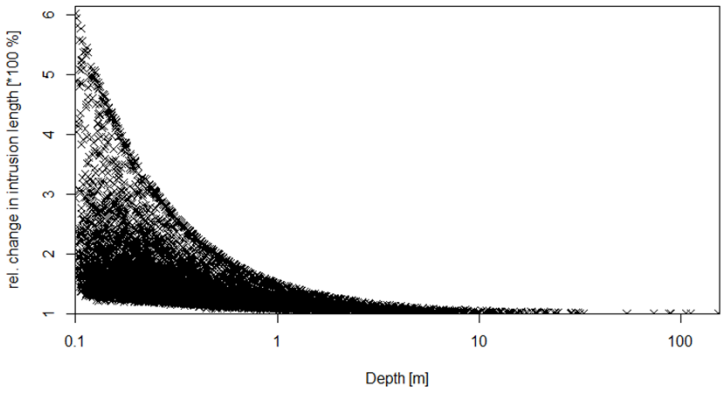

Figure 14: Relation of expected increase in saltwater intrusion length with sea level rise in regard to original delta depth.

3.4.3 Sea level rise and discharge change combined

The combined effect of changes in both discharge and sea level has a higher magnitude of change than changes in discharge alone (compare Fig. 10 & 15). Next to the previously identified increases in intrusion length in Central America, the Mediterranean stands out as a region where intrusion lengths are expected to more than double. Additionally, the US Atlantic Coast and Eastern Asia have especially high and regionally consistent projected change. Globally, the vast majority of deltas are here projected to experience increasing saltwater intrusion, while it decreases just for a minority of deltas. The deltas with the smallest changes can be localized in North-East Brazil, Scandinavia or the US Pacific Coast.

The combined effect of changes in sea level rise and discharge is dominated by changes in the former (Fig. 16). While a change in discharges alone lead to an average decrease of intrusion lengths, sea level rise leads globally to a substantial increase of saltwater intrusion. This effect is mainly present for deltas in the lowest 90 % of intrusion lengths, while the deltas which already had high intrusion lengths in current conditions are less impacted.

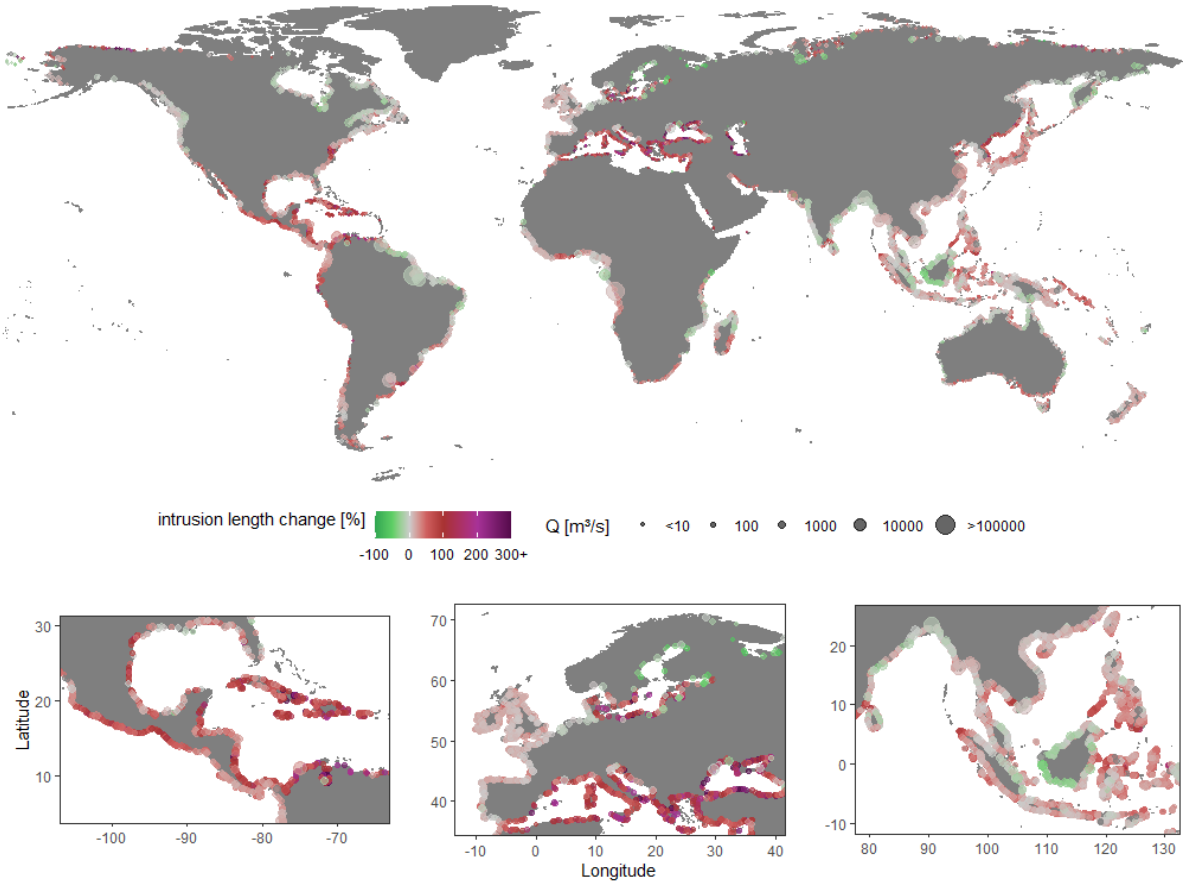

Figure 15: Map of intrusion length change in a future climate scenario with sea level rise.

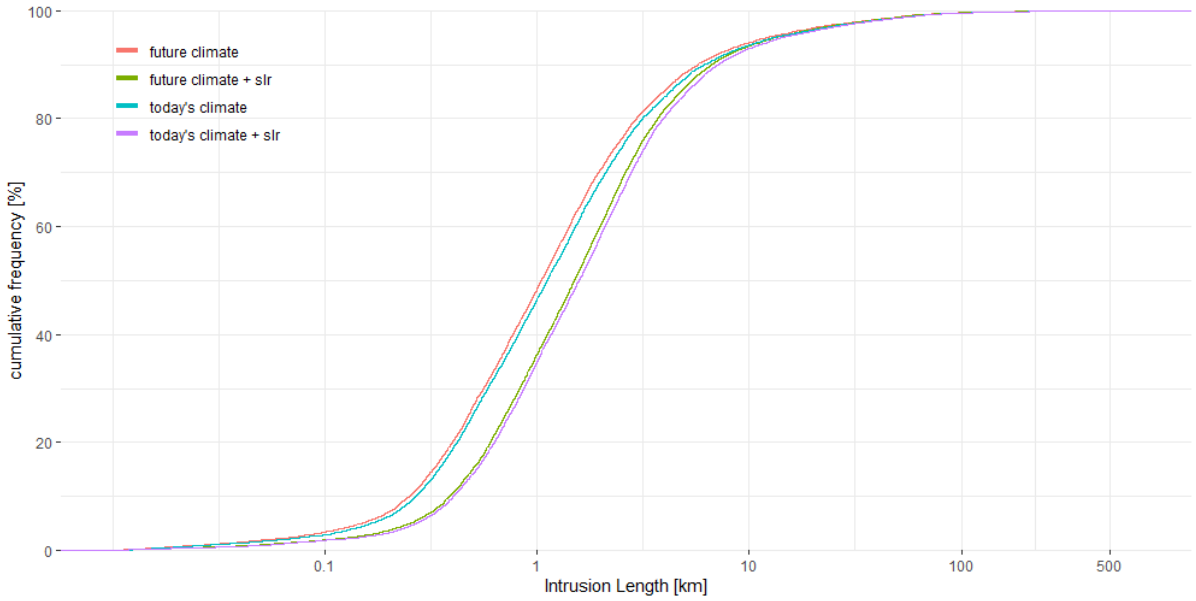

Figure 16: Cumulative frequency distribution of occurring saltwater intrusion lengths for current and future climate with and without sea level rise ("slr" in legend).

4 Discussion

4.1 Saltwater intrusion and impacts

4.1.1 Current saltwater intrusion

For the first time, this study estimated saltwater intrusion on a global scale. The model was able to identify hotspot regions where high saltwater intrusion occurs. These are well in line with reports saltwater intrusion, as for example for the Yangtze estuary (Cai *et al.*, 2015), Mekong (Toan, 2014), Bay of Bengal (Allison *et al.*, 2003) or the Vu Gia – Thu Bon in Vietnam (Nga *et al.*, 2020). Those are all located in South-East Asia which was found to be one of the regions with many deltas estimated to have a high intrusion length by the used model. While the comparison of the actual intrusion length is not promising due to the limitations and inaccuracies of the model (Fig. 3 & Ch. 4.2) the existing reports indicate that saltwater intrusion is an impactful issue in these regions. A comparison of the model with the hotspots identified in these field studies suggests that the model differentiates well between regions of low and high intrusion.

According to the model, high saltwater intrusion occurs mainly in deltas with a large mouth width, length scale or tidal amplitude. This is supported by the sensitivity analysis, which shows that these three parameters lead to an increase in intrusion length. Thus, large deltas can generally be expected to have a higher saltwater intrusion length. This naturally still depends on discharge. Many deltas can be found in the northern hemisphere that are relatively large in relation to their discharge, which originates from their morphology dating back to glacial periods with high amount of discharge due to snow and glacial melt. In the model, many of these deltas are shown to have high intrusion lengths, exemplarily at the Bay of Hudson, Sea of Okhotsk or the coast of Alaska. However, and most likely due to the low population and low dependence on estuary freshwater, no studies about the saltwater intrusion length in these regions could be found.

The calibration is also based only on deltas with an assumed width below 1 km (Tab. 3). The high intrusion lengths calculated for large deltas might thus also be related to scaling issues and the lack of consideration of very wide or long deltas during calibration.

Overall, the absolute values of intrusion length are estimated to be low for many deltas (50 % of deltas with $L^{HWS} < 1$km, 92 % with $L^{HWS} < 10$ km, Ch. 3.2). While validation on a global scale is lacking (see Ch. 4.2.1), the calculated intrusion lengths are for the majority cases too low compared to available measurements (Fig. 3). Hence, it can be assumed that these absolute intrusion length values are generally underestimated but with the used approach a further evaluation is not possible.

4.1.2 Future saltwater intrusion and its potential impacts

Despite the explained limitations of this saltwater intrusion model, the depicted results still give an indication about the expected development of saltwater intrusion in the future. The absolute values may not be the most indicative, but the expected change in regard to discharge should be quite reliable, since the sensitivity of the model to discharge is quite clear and on a similar scale for all calibration variants. The strong relation of salt intrusion to discharge is also reported by Zhang *et al.* (2010).

Projected changes in average discharge and respective changes in salt intrusion length indicate, that estuaries which currently experience high intrusion lengths, are not likely to expect high changes in average intrusion lengths. However, some regions with high populations and extensive agricultural production are expected to have increased intrusion lengths compared to current conditions. This applies especially to Western Africa and a large part of South-East Asia. Further and more detailed research on saltwater intrusion in these regions is recommended, particularly in view of a growing population and increasing water demands (e.g. Rosegrant *et al.*, 2009).

Projected high changes are not necessarily related to an increasing problem of delta salinization. The shown relative changes often occur in small deltas, which also have small intrusion lengths. While an estimation of the impacts requires a closer look at the regional conditions of water usage, the direct impact on freshwater use is postulated to be low. However, these changes might have significant ecological impacts due increased salinization and an incidental expansion of the brackish water zone in estuary. In the case of wetland plant and tree species, the raised salinity levels can cause salt stress, compromised growth, and increased mortality, potentially leading to an irreversible forest degradation in many wetlands (Day *et al.*, 2007; Ardón *et al.*, 2013). Saltwater intrusion additionally restricts the nitrogen retaining function of freshwater wetland soils, resulting in an elevated nitrogen export and subsequently higher nitrogen levels in the sensitive coastal ecosystems (Ardón *et al.*, 2013). Furthermore, aquatic organisms accustomed to the freshwater environment are not adapted to the increased salinity levels. The ensuing reduction in biodiversity will puts constraints on important ecosystem services (Cañedo-Argüelles *et al.*, 2013). The combined complex effects of salt intrusion through both natural saltwater incursion and adverse land use decisions certainly complicates the isolated assessment of climate change impacts on the salinization and degradation of these ecosystems (Ardón *et al.*, 2013).

The presented results also indicate that the effect of sea level rise is, globally averaged, a lot higher than the effects of the change in discharge (Fig. 10 & 13). This is induced by sea level rise highly affecting small deltas in this model where a change in depth 0.5 m represents a high relative change in total depth (Fig. 14). For the large deltas, sea level rise induced change of intrusion length is comparably small. This might vary though, since Toan (2014) exemplarily estimated an increase of intrusion length of 20 to 27 km compared to present conditions for the Mekong delta, in regard to a sea level rise of 1 m. The used MIKE11 model in that study allows for a much more detailed analysis and considers the elevation and respective flooding of the area due to a higher sea level. This cannot be considered in the simple analytical model used in this

study. Generally, coastlines are going to retreat due to sea level rise, even though there is currently uncertainty about the magnitude of change (Ranasinghe & Stive, 2009). Lower discharges on global average will probably increase intrusion of tidal water and also lead to a rise of sediment transport into deltas (Nienhuis *et al.*, 2018). Thus, delta outlets are likely to also move further inland compared to their current position and delta geometry in terms of width and length is expected to adjust. The here projected increase in intrusion does not take these changes in morphology into account. It gives an indication about where intrusion could increase but more detailed analysis which takes morphologic changes into account is required to make better local predictions and an impact assessment.

Limited freshwater availability from estuaries leads to the need for alternative water sources. Groundwater is a common substitute and is used especially often for irrigation (Giordano, 2009). Globally, environmental flow conditions for many groundwater sources are expected to be reached within the next century, with respective impacts on aquatic ecology and subsequently also economy (de Graaf *et al.*, 2019). Groundwater resources are hence globally not a sustainable long-term alternative to freshwater from estuaries, especially not since coastal aquifers are expected to have an increase in salinity as well (e.g. Essink, 1999; Sherif & Singh, 1999; Werner & Simmons, 2009). This phenomenon, which is usually also referred to as "coastal saltwater intrusion" is easy to confuse with the saltwater intrusion into estuaries and is more abundant in literature. Sea level rise is the main reason for salinization of coastal aquifers. However, the effects are regionally also quite different and depend on local hydrology. For example, Sherif & Singh (1999) estimate an increase of intrusion length in coastal aquifers of 0.4 km in the Bay of Bengal, but of 9 km in the Nile Delta for a sea level rise of 0.5 m.

Increasing salinity in deltas requires cost-intensive desalination plants to lower the salinity level. Bhuiyan & Dutta (2011) recommend a regulation of river flow for southwestern Bangladesh. By that, low-flows could be avoided and discharge levels potentially kept high enough to push sufficiently against intruding saline water. In low-income countries, an appropriate treatment as such might not be feasible and the potential impacts on human health must be faced (Vineis *et al.*, 2011). A main impact of high salt intake through drinking water on human health is the increase of blood pressure which can lead to strokes and other cardiovascular diseases (Calabrese & Tuthill, 1981; He & MacGregor, 2007).

4.2 Model Quality

4.2.1 Reproducing historic conditions and model validation

Reproducing historic conditions has been of moderate success, with the best obtained fit having an R^2 of 0.51 between model output and measurements. This highly deviates from the good results obtained by Savenije (1993) who used, next to local measurements for estuary geometry, also case specific measurements for tidal amplitude (here: delta-specific constant) and the tidal excursion, which had to be regarded as a global constant here in the absence of field data. While the tidal excursion can be on average reasonably approximated with 14 km (Savenije, 2012) compared to 12.2 ±5.1 km for the 45 cases by Savenije (1993),

the latter still shows quite some variation which cannot be measured. Approaches to predict the tidal excursion exist but are too complex and require too much input data to apply them on a global scale (e.g. Parsa & Shahidi, 2010).

The results of the model highly depend on calibration. Re-calibration of the original model by Savenije (1993) shows very different results depending on the used "first-guess" coefficients during optimisation. The here used optimisation algorithm has difficulties finding a global optimum due to the optimal coefficients being on very different scales (see Ch. 3.2). Hence, using different sets of first-guess coefficients has been required to find a better calibration. This could potentially be bypassed by using a better algorithm for global optimisation over different parameters.

The limited optimisation lead to an improvement in predictive capability of the historic conditions with *K* values in a realistic and usable range. Together with the relative closeness to the original, physically reasoned, calibration, this calibration is presumably still physically based. In contrast, the full optimisation lead to *K* values below 0.06 which still allows their usage but is very low compared to the common more uniform distribution of values between 0 and 1. This indicates a less physical meaning of *K* and the entire calibration which is supported by a less sensitive model to input parameters but higher salt intrusion results overall. Obtained *K* values differentiate substantially from the values Savenije (1993) gives for the same estuaries. This originates from the very different geometric description which can be seen when comparing delta parameters in Tables 3 and 4. The same delta is essentially very differently characterized between the datasets so that the *K* values also deviate.

Using a Monte-Carlo simulation to find optimal coefficients lead to a large (1000+) amount of possible coefficient combinations resulting in an almost identical best RMSE value. This occurs mainly due to the balancing between factors f_K and f_α. The coefficients eventually chosen as the optimum, represent the lowest obtained RMSE, however, the differences between coefficient sets were so small (RMSE error differences on the scale of 10^{-5}) that these might originate from numerical uncertainties and a different set of coefficients could equally be used here. This problem of equifinality emphasizes the pure statistical fit of the model, but a lack of physical reasoning.

Validation is a crucial component of hydrological modelling (Biondi *et al.*, 2012) and would be very beneficial to improve modelling of saltwater intrusion in deltas. Currently, there is no global database about saltwater intrusion length or estuary salinity. Existing case studies and individual data sources can potentially be used to calibrate against. However, their generalisability remains limited. An exploratory attempt, by using available salinity, respectively electrical conductivity, data was conducted. Due to limited data along the coasts, the new dataset of Thorslund & van Vliet (2020) did not contain enough datapoints for a sufficient estimation of saltwater intrusion lengths. Spatially, measurement stations are often placed dozens of kilometres apart from each other, preventing the recognition of a clear maximum distance of saltwater intrusion. Temporally, these stations often give only daily or monthly averages of salinity. While other measures as discharge can be assumed to be relatively constant over a day or month, salinity is steadily

varying in an estuary due to tidal flow. A temporal average hence dilutes the maximum salinity value reached. Published data about intrusion length measurements (e.g. Savenije, 2012; Gisen *et al.,* 2015; Zhang & Savenije, 2019) or parameters related to estuarine dynamics or geometry (Toffolon *et al.*, 2006) usually consist of river or delta names in conjunction with parameter values. Intrusion length measurements are usually taken for very specific events like the maximum intrusion during a particular tidal cycle and are no long-term measurements. This originates from the problem, that the required resolution is difficult to obtain and hence boat surveys, performed along high water travelling inlands, are recommended (Savenije, 2012). As remarked in the data preparation for re-calibration (Ch. 2.2), the definition of the outlet of a delta or estuary is not standardised, leading to an offset of delta mouth location between datasets. This propagates respectively to reported saltwater intrusion length and mentioned issues in transferability between datasets. Therefore, it is here recommended to include more spatial information when publishing information about measurements in estuaries.

4.2.2 Salt intrusion length modelling

The saltwater intrusion length gives a value for the maximum distance saltwater can travel. Although this distance is a good first indicator for the magnitude and potential severity of saltwater intrusion at a location, even if saltwater can reach a place where freshwater is needed, the salt concentration may still be too low to have noticeable impacts. This deduction would require a spatial estimate of the salinity. The profile of the salinity curve can highly vary depending on the river estuary shape, leading to salt intrusion curves ranging from a recession to dome shape and even humpback shape if certain conditions apply (Savenije, 2012). The available data quality is not sufficient to make a valid assessment of the estuary shape and requires a more individual analysis.

The actual process of tidal intrusion and the mixing of saltwater and freshwater has not been directly covered in this study since the focus was laid on the global application of an existing model. At this point though, it needs to be pointed out that intrusion and mixing are very complex processes which are described in detail in Savenije (2012). He differentiates between three main mixing processes which are *(i)* vertical and horizontal circulation induced by wind, *(ii)* gravitational circulation due to density differences between saline water and freshwater *(iii)* turbulent mixing and tidal shear among other types of mixing which all originate from the kinetic energy provided by the tide. The prevalence of these mixing types depends largely on the intensity of the tides and the geometry of the delta. This shall emphasize the general difficulty of representing all these processes in one simple analytical model. While the here used model is supposed to work on various types of estuaries (Savenije, 1993), later publications of the author indicate that a differentiation of model use depending on estuary characteristics might be favourable and lead to better results (Zhang & Savenije, 2019).

4.2.3 Data

A crucial part of the presented saltwater intrusion model is an accurate description of estuary geometry. Instead of local measurements, the here used geometry originates from a morphological model (Nienhuis *et al.*, 2018, 2020). Due to the simplicity of the model, it does not consider sediment characteristics, which are fundamental for the delta shape, and does not include any anthropogenic overprint. The latter is especially relevant in highly populated areas which are most vulnerable to reduced freshwater resources by increased salinity. Delta geometry and tidal parameters form Van der Burgh's *K*, which is an important delta characteristic for this model. Savenije (1993) recommends to calibrate for this parameter and only use his approach for estimation (eq. 3) in exceptional cases when no data for calibration is available. Since this is generally the case for global modelling, his approach has been used here. Zhang & Savenije (2019) propose a further simplified estimation of Van den Burgh's *K* by using proportionality between *K* and the logarithm of the quotient of estuary length and mouth width and therewith reducing the required parameters to length and width. However, they do not quantify this relationship and due to the generally low estuary length values in the here used dataset and missing data for calibration this approach could here not be further pursued.

The model of Savenije (1993) assumes a deltaic shape which can be expressed by an exponential function for width and length convergence. In contrast, Nienhuis *et al.* (2018) consider a prismatic delta shape and just a single scale for the delta convergence. Furthermore, Savenije (1993) allows the expression of convergence into two separate parts, which allows for a better representation of the estuary shape. In those cases, the formula of saltwater intrusion is adjusted. This part of the intrusion had to be excluded in this study since the global delta dataset does not include information about the delta shape.

Using output of a global morphological model as input for the here applied saltwater intrusion is not optimal, since that model already introduces a lot of uncertainty. Exemplarily, the definition of the delta mouth depth amounting of $1/100^{th}$ of the delta mouth width, appears to be a clear simplification prone to errors. Also, as a morphological model, Nienhuis *et al.* (2018) consider only the natural development of a delta but not possible human or ecosystem induced change of deltaic shape. This is particularly relevant since deltas are often highly populated which can lead to an altered estuary shape to create favourable space for cities or agricultural areas.

An alternative data source for estuary geometry should be highly considered when performing global saltwater intrusion modelling in the future. There is no clear separation between the terms "delta" and "estuary" but large indifferences in related geometric parameters indicate that different definitions are used here. Preferably, delta geometry should rely on measurements and not on morphological models. Remote sensing-based surveying could here improve the shape definition and should be further considered.

The quality of the discharge input was not evaluated as part of this study. However, compared to the uncertainties introduced by the definition model itself, and the inaccuracies in delta geometry, discharge is assumed to be a minor source of uncertainty at the current state of global saltwater intrusion modelling.

While measurements would here also be favourable, especially for calibration, those are not available around the globe. Hence, the here used and well validated output from Sutanudjaja *et al.* (2018) can be rated as sufficient.

4.3 Outlook

Future global saltwater intrusion research could greatly benefit from a better-defined global dataset of estuary shapes and an improvement of the intrusion model itself. The here used model was already introduced in 1993 and has hence been improved (e.g. Savenije, 2012; Gisen *et al.*, 2015; Zhang & Savenije, 2019). However, those advancements require often more input data or are just applicable for a certain type of data with a prevalent type of mixing between sea- and freshwater. The available models are hence all not very suitable for application on a global scale and could potentially be further improved in regards of the needs of global modelling. This should specifically target the data available on the global scale and be universally applicable on all kind of deltas.

For future research of impacts of saltwater intrusion into deltas, it is recommended to put a higher emphasis on actual water demand. Specifically, irrigation demand varies seasonally and hydrological extremes like droughts might amplify the requirement of freshwater from estuaries. Exemplarily, Sun *et al.* (2009) define September to November as critical season for ecological salinity objects for the Yangtze estuary. This period is not the period with the lowest discharges in a year. At the same time, discharge can significantly vary seasonally due to different prevailing hydrological regimes. For the Mekong river, Toan (2014) reports a minimum of river flow during the months of March and April with negative impacts for water supply for human consumption and agricultural cultivation.

Global discharge is well modelled and output is readily available on a daily time scale which allows for an assessment of seasonal differences in discharge and hence intrusion lengths (e.g. Sutanudjaja *et al.*, 2018). Ensemble modelling of discharge also makes an analysis of the re-occurrence and severity of extreme low flows and hence high salinity levels in estuaries possible. Van der Wiel *et al.* (2019) have presented a global discharge ensemble dataset for current and warmer climate conditions, which is promising for this application. While further improvement of the saltwater intrusion model and the creation of a different dataset for delta shape will take some time, the discharge data availability makes analysis of seasonal differences in estuary salinity and extreme conditions already achievable.

5 Conclusion

The aim of this study was to perform a first analysis of saltwater intrusion into deltas on a global scale and analyse its predictive quality and applicability. Therefore, an existing analytical model for saltwater intrusion was used with global datasets of modelled delta shapes and locations, tidal conditions, and freshwater discharge.

The results show that the model is well capable of identifying reported regions with a high saltwater intrusion, particularly South-East Asia, but has limitations in giving reliable absolute values of intrusion length. The model outcome highly depends on adequate calibration which is currently difficult to conduct since appropriate salt intrusion measurements are rare which also inhibits model validation. Generally, the available input of global delta and in particular of delta geometry has been assessed as not yet satisfying and improvement here could probably enhance the quality of future research about global saltwater intrusion.

Projected changes of discharge at the end of the 21st century suggest that the global average of saltwater intrusion lengths will decrease. However, there are strong regional differences of estimated change. While deltas with a nowadays high intrusion are not expected change much, other regions may experience higher salinity levels in their deltas which require further local analysis. The same applies to sea level rise, which appears to have the most impact on small deltas even though this might originate from the type of implementation of sea level rise here conducted.

This study gives a first indication about global distribution of saltwater intrusion which can be well used in studies about freshwater resources for agricultural cultivation or human consumption and degradation of coastal ecosystems. It also allows for more impact-focused research in the future, where readily available discharge simulations could be used to assess temporal differences in saltwater intrusion. These could then be combined with actual water demands to better evaluate the severity of saltwater intrusion in deltas around the word and steer potential counter measures.

References

Aerts, J.C.J.H., **Hassan, A.**, **Savenije, H.H.G.** and **Khan, M.F.** (2000) Using GIS tools and rapid assessment techniques for determining salt intrusion: STREAM, a river basin management instrument. *Phys. Chem. Earth, Part B Hydrol. Ocean. Atmos.*, **25**, 265–273.

Allison, M.A., **Khan, S.R.**, **Goodbred, J.L.** and **Kuehl, S.A.** (2003) Stratigraphic evolution of the late Holocene Ganges-Brahmaputra lower delta plain. *Sediment. Geol.*, **155**, 317–342.

Amante, C. and **Eakins, B.W.** (2009) ETOPO1 1 Arc-Minute Global Relief Model: Procedures, Data Sources and Analysis. *NOAA Tech. Memo. NESDIS NGDC-24*, 19.

Ardón, M., **Morse, J.L.**, **Colman, B.P.** and **Bernhardt, E.S.** (2013) Drought-induced saltwater incursion leads to increased wetland nitrogen export. *Glob. Chang. Biol.*, **19**, 2976–2985.

Bhuiyan, M.J.A.N. and **Dutta, D.** (2011) Control of salt water intrusion due to sea level rise in the coastal zone of Bangladesh. *WIT Trans. Ecol. Environ.*, **149**, 163–173.

Biondi, D., **Freni, G.**, **Iacobellis, V.**, **Mascaro, G.** and **Montanari, A.** (2012) Validation of hydrological models: Conceptual basis, methodological approaches and a proposal for a code of practice. *Phys. Chem. Earth*, **42–44**, 70–76.

Buschman, F.A., **Hoitink, A.J.F.**, **Van Der Vegt, M.** and **Hoekstra, P.** (2010) Subtidal flow division at a shallow tidal junction. *Water Resour. Res.*, **46**, 1–12.

Cai, H., **Savenije, H.H.G.** and **Toffolon, M.** (2014) Linking the river to the estuary: Influence of river discharge on tidal damping. *Hydrol. Earth Syst. Sci.*, **18**, 287–304.

Cai, H., **Savenije, H.H.G.**, **Zuo, S.**, **Jiang, C.** and **Chua, V.P.** (2015) A predictive model for salt intrusion in estuaries applied to the Yangtze estuary. *J. Hydrol.*, **529**, 1336–1349.

Calabrese, E.J. and **Tuthill, R.W.** (1981) The influence of elevated levels of sodium in drinking water on elementary and high school students in Massachusetts. *Sci. Total Environ.*, **18**, 117–133.

Cañedo-Argüelles, M., **Hawkins, C.P.**, **Kefford, B.J.**, **Schäfer, R.B.**, **Dyack, B.J.**, **Brucet, S.**, **Buchwalter, D.**, **Dunlop, J.**, **Frör, O.**, **Lazorchak, J.**, **Coring, E.**, **Fernandez, H.R.**, **Goodfellow, W.**, **Achem, A.L.G.**, **Hatfield-Dodds, S.**, **Karimov, B.K.**, **Mensah, P.**, **Olson, J.R.**, **Piscart, C.**, **Prat, N.**, **Ponsá, S.**, **Schulz, C.J.** and **Timpano, A.J.** (2016) Saving freshwater from salts : Ion-specific standards are needed to protect biodiversity. *Science (80-.).*, **351**, 914–916.

Cañedo-Argüelles, M., **Kefford, B.J.**, **Piscart, C.**, **Prat, N.**, **Schäfer, R.B.** and **Schulz, C.J.** (2013) Salinisation of rivers: An urgent ecological issue. Environ. Pollut. **173**:157–167.

Church, J. a., **Clark, P.U.**, **Cazenave, A.**, **Gregory, J.M.**, **Jevrejeva, S.**, **Levermann, A.**, **Merrifield, M. a.**, **Milne, G. a.**, **Nerem, R..**, **Nunn, P.D.**, **Payne, A.J.**, **Pfeffer, W.T.**, **Stammer, D.** and **Unnikrishnan, A.S.** (2013) Sea level change. *Clim. Chang. 2013 Phys. Sci. Basis. Contrib. Work. Gr. I to Fifth Assess. Rep. Intergov. Panel Clim. Chang.*, 1137–1216.

Dai, A. (2011) Drought under global warming: A review. Wiley Interdiscip. Rev. Clim. Chang. 2:45–65.

Dai, A. (2013) Increasing drought under global warming in observations and models. *Nat. Clim. Chang.*, **3**, 52–58.

Day, R.H., **Williams, T.M.** and **Swarzenski, C.M.** (2007) Hydrology of Tidal Freshwater Forested Wetlands of the Southeastern United States. In: *Ecology of Tidal Freshwater Forested Wetlands of the Southeastern United States*, *Springer Netherlands*, Dordrecht, 29–63.

de Graaf, I.E.M., **Gleeson, T.**, **van Beek, L.P.H.**, **Sutanudjaja, E.H.** and **Bierkens, M.F.P.** (2019) Environmental flow limits to global groundwater pumping. *Nature*, **574**, 90–94.

Doan, Q.T., **Nguyen, C.D.**, **Chen, Y.C.** and **Pawan, K.M.** (2014) Modeling the influence of river flow

and salinity intrusion in the Mekong River Estuary, Vietnam. *Lowl. Technol. Int.*, **16**, 14–25.

Dufresne, J.L., **Foujols, M.A.**, **Denvil, S.**, **Caubel, A.**, **Marti, O.**, **Aumont, O.**, **Balkanski, Y.**, **Bekki, S.**, **Bellenger, H.**, **Benshila, R.**, **Bony, S.**, **Bopp, L.**, **Braconnot, P.**, **Brockmann, P.**, **Cadule, P.**, **Cheruy, F.**, **Codron, F.**, **Cozic, A.**, **Cugnet, D.**, **de Noblet, N.**, **Duvel, J.P.**, **Ethé, C.**, **Fairhead, L.**, **Fichefet, T.**, **Flavoni, S.**, **Friedlingstein, P.**, **Grandpeix, J.Y.**, **Guez, L.**, **Guilyardi, E.**, **Hauglustaine, D.**, **Hourdin, F.**, **Idelkadi, A.**, **Ghattas, J.**, **Joussaume, S.**, **Kageyama, M.**, **Krinner, G.**, **Labetoulle, S.**, **Lahellec, A.**, **Lefebvre, M.P.**, **Lefevre, F.**, **Levy, C.**, **Li, Z.X.**, **Lloyd, J.**, **Lott, F.**, **Madec, G.**, **Mancip, M.**, **Marchand, M.**, **Masson, S.**, **Meurdesoif, Y.**, **Mignot, J.**, **Musat, I.**, **Parouty, S.**, **Polcher, J.**, **Rio, C.**, **Schulz, M.**, **Swingedouw, D.**, **Szopa, S.**, **Talandier, C.**, **Terray, P.**, **Viovy, N.** and **Vuichard, N.** (2013) Climate change projections using the IPSL-CM5 Earth System Model: From CMIP3 to CMIP5. 2123–2165.

Egbert, G.D. and **Erofeeva, S.Y.** (2002) Efficient Inverse Modeling of Barotropic Ocean Tides. *J. Atmos. Ocean. Technol.,* **19**, 183–204

Ericson, J.P., **Vörösmarty, C.J.**, **Dingman, S.L.**, **Ward, L.G.** and **Meybeck, M.** (2006) Effective sea-level rise and deltas: Causes of change and human dimension implications. *Glob. Planet. Change*, **50**, 63–82.

Essink, G.H.P.O. (1999) Impact of Sea Level Rise in the Netherlands. In: *Seawater Intrusion in Coastal Aquifers --- Concepts, Methods and Practices* (Ed. J. Bear, A.H.-D. Cheng, S. Sorek, D. Ouazar, and I. Herrera), *Springer Netherlands*, Dordrecht, 507–530.

Giordano, M. (2009) Global groundwater? Issues and solutions. *Annu. Rev. Environ. Resour.*, **34**, 153–178.

Gisen, J.I.A., **Savenije, H.H.G.** and **Nijzink, R.C.** (2015) Revised predictive equations for salt intrusion modelling in estuaries. *Hydrol. Earth Syst. Sci.*, **19**, 2791–2803.

Haddeland, I., **Heinke, J.**, **Biemans, H.**, **Eisner, S.**, **Flörke, M.**, **Hanasaki, N.**, **Konzmann, M.**, **Ludwig, F.**, **Masaki, Y.**, **Schewe, J.**, **Stacke, T.**, **Tessler, Z.D.**, **Wada, Y.** and **Wisser, D.** (2014) Global water resources affected by human interventions and climate change. *Proc. Natl. Acad. Sci.*, **111**, 3251–3256.

He, F.J. and **MacGregor, G.A.** (2007) Salt, blood pressure and cardiovascular disease. *Curr Opin Cardiol*; **22**(4),298–305.

Huu-Thoi, N. and **Gupta, A. Das** (2001) Assessment of water resources and salinity intrusion in the mekong delta. *Water Int.*, **26**, 86–95.

Kaushal, S.S., **Likens, G.E.**, **Pace, M.L.**, **Utz, R.M.**, **Haq, S.**, **Gorman, J.** and **Grese, M.** (2018) Freshwater salinization syndrome on a continental scale. *Proc. Natl. Acad. Sci.*, **115**, E574–E583.

Lehner, B., **Verdin, K.** and **Jarvis, A.** (2008) New global hydrography derived from spaceborne elevation data. *Eos (Washington. DC).*, **89**, 93–94.

Nga, T.T., **Cong, V.H.** and **Hung, L.** (2020) Assessing the Impacts of Climate Change and Reservoir Operation on Saltwater Intrusion in the Vu Gia - Thu Bon River Basin. In: *APAC 2019*, *Springer Singapore*, Singapore, 1207–1212.

Nguyen, A.D. and **Savenije, H.H.G.** (2006) Salt intrusion in multi-channel estuaries: A case study in the Mekong Delta, Vietnam. *Hydrol. Earth Syst. Sci.*, **10**, 743–754.

Nienhuis, J.H. (2020) Personal Communication.

Nienhuis, J.H., **Ashton, A.D.**, **Edmonds, D.A.**, **Hoitink, A.J.F.**, **Kettner, A.J.**, **Rowland, J.C.** and **Törnqvist, T.E.** (2020) Global-scale human impact on delta morphology has led to net land area gain. *Nature*, **577**, 514–518.

Nienhuis, J.H., **Hoitink, A.J.F.T.** and **Törnqvist, T.E.** (2018) Future Change to Tide-Influenced Deltas. *Geophys. Res. Lett.*, **45**, 3499–3507.

Noe, G.B., **Krauss, K.W.**, **Lockaby, B.G.**, **Conner, W.H.** and **Hupp, C.R.** (2013) The effect of increasing salinity and forest mortality on soil nitrogen and phosphorus mineralization in tidal freshwater forested wetlands. *Biogeochemistry*, **114**, 225–244.

Parsa, J. and **Shahidi, A.E.** (2010) Prediction of tidal excursion length in estuaries due to the environmental changes. *Int. J. Environ. Sci. Technol.*, **7**, 675–686.

Pont, D., **Day, J.W.**, **Hensel, P.**, **Franquet, E.**, **Torre, F.**, **Rioual, P.**, **Ibànez, C.** and **Coulet, E.** (2002) Response scenarios for the deltaic plain of the Rhône in the face of an acceleration in the rate of sea-level rise with special attention to Salicornia-type environments. *Estuaries*, **25**, 337–358.

Prudhomme, C., **Giuntoli, I.**, **Robinson, E.L.**, **Clark, D.B.**, **Arnell, N.W.**, **Dankers, R.**, **Fekete, B.M.**, **Franssen, W.**, **Gerten, D.**, **Gosling, S.N.**, **Hagemann, S.**, **Hannah, D.M.**, **Kim, H.**, **Masaki, Y.**, **Satoh, Y.**, **Stacke, T.**, **Wada, Y.** and **Wisser, D.** (2014) Hydrological droughts in the 21st century, hotspots and uncertainties from a global multimodel ensemble experiment. *Proc. Natl. Acad. Sci. U. S. A.*, **111**, 3262–3267.

R Core Team (2020) R: A Language and Environment for Statistical Computing.

Rahman, M.M., **Penny, G.**, **Mondal, M.S.**, **Zaman, M.H.**, **Kryston, A.**, **Salehin, M.**, **Nahar, Q.**, **Islam, M.S.**, **Bolster, D.**, **Tank, J.L.** and **Müller, M.F.** (2019) Salinization in large river deltas: Drivers, impacts and socio-hydrological feedbacks. *Water Secur.*, **6**, 100024.

Ranasinghe, R. and **Stive, M.J.F.** (2009) Rising seas and retreating coastlines. *Clim. Change*, **97**, 465–468.

Rosegrant, M.W., **Ringler, C.** and **Zhu, T.** (2009) Water for agriculture: Maintaining food security under growing scarcity. *Annu. Rev. Environ. Resour.*, **34**, 205–222.

Savenije, H.H.G. (2012) Salinity and tides in alluvial estuaries, 2nd edn. 163 pp.

Savenije, H.H.G. (1993) Predictive model for salt intrusion in estuaries. *J. Hydrol.*, **148**, 203–218.

Savenije, H.H.G. (2015) Prediction in ungauged estuaries: An integrated theory. *Water Resour. Res.*, **51**, 2464–2476.

Savenije, H.H.G. Salinity and tides in alluvial estuaries. https://salinityandtides.com/applications/. Accessed 20 Jul 2020

Sherif, M.M. and **Singh, V.P.** (1999) Effect of climate change on sea water intrusion in coastal aquifers. *Hydrol. Process.*, **13**, 1277–1287.

Sun, T., **Yang, Z.F.**, **Shen, Z.Y.** and **Zhao, R.** (2009) Environmental flows for the Yangtze Estuary based on salinity objectives. *Commun. Nonlinear Sci. Numer. Simul.*, **14**, 959–971.

Sutanudjaja, E.H., **Beek, R. Van**, **Wanders, N.**, **Wada, Y.**, **Bosmans, J.H.C.**, **Drost, N.**, **Ent, R.J. Van Der**, **Graaf, I.E.M. De**, **Hoch, J.M.**, **Jong, K. De** and **Karssenberg, D.** (2018) PCR-GLOBWB 2 : a 5 arcmin global hydrological and water resources model. *Geosci. Model Dev.*, **11**, 2429–2453.

Syvitski, J.P.M. and **Saito, Y.** (2007) Morphodynamics of deltas under the influence of humans. *Glob. Planet. Change*, **57**, 261–282.

Thorslund, J. and **van Vliet, M.T.H.** (2020) A global dataset of surface water and groundwater salinity measurements from 1980–2019. *Sci. Data*, **7**, 1–11.

Toan, T.Q. (2014) Climate Change and Sea Level Rise in the Mekong Delta: Flood, Tidal Inundation, Salinity Intrusion, and Irrigation Adaptation Methods. In: *Coastal Disasters and Climate Change in Vietnam: Engineering and Planning Perspectives*, *Elsevier Inc.*, 199–218.

Toffolon, M., **Vignoli, G.** and **Tubino, M.** (2006) Relevant parameters and finite amplitude effects in estuarine hydrodynamics. *J. Geophys. Res. Ocean.*, **111**, 1–17.

UNEP (2016) A Snapshot of the World's Water Quality: Towards a global assessment. Nairobi, Kenya,

162 pp.

Van der Burgh, P. (1972) Ontwikkeling van een methode voor her voorspellen van zoutverde- lingen in estuaria, kanalen en zeeen. In: *Rijkswaterstaat Rapport*, 10–72.

van der Wiel, K., **Wanders, N.**, **Selten, F.M.** and **Bierkens, M.F.P.** (2019) Added value of large ensemble simulations for assessing extreme river discharge in a 2 ° C warmer world. Geophys Res Lett., **46**, 2093– 2102

Vineis, P., **Chan, Q.** and **Khan, A.** (2011) Climate change impacts on water salinity and health. J. Epidemiol. Glob. Health **1**, 5–10.

Wanders, N. and **Van Lanen, H.A.J.** (2015) Future discharge drought across climate regions around the world modelled with a synthetic hydrological modelling approach forced by three general circulation models. *Nat. Hazards Earth Syst. Sci.*, **15**, 487–504.

Werner, A.D. and **Simmons, C.T.** (2009) Impact of sea-level rise on sea water intrusion in coastal aquifers. *Ground Water*, **47**, 197–204.

Zhang, E., **Savenije, H.H.G.**, **Wu, H.**, **Kong, Y.** and **Zhu, J.** (2011) Analytical solution for salt intrusion in the Yangtze Estuary, China. *Estuar. Coast. Shelf Sci.*, **91**, 492–501.

Zhang, W., **Feng, H.**, **Zheng, J.**, **Hoitink, A.J.F.T.** and **van der Vegt, M.** (2013) Numerical Simulation and Analysis of Saltwater Intrusion Lengths in the Pearl River Delta, China. *J. Coast. Res.*, **29**, 372–382.

Zhang, Z., **Cui, B.**, **Zhao, H.**, **Fan, X.** and **Zhang, H.** (2010) Discharge-salinity relationships in Modaomen waterway, Pearl River estuary. *Procedia Environ. Sci.*, **2**, 1235–1245.

Zhang, Z. and **Savenije, H.** (2019) Maximum power of saline and fresh water mixing in estuaries. *Earth Syst. Dynam*, **10**, 667–684.

Statement of originality of the MSc thesis

I declare that:

1. this is an original report, which is entirely my own work,

2. where I have made use of the ideas of other writers, I have acknowledged the source in all instances,

3. where I have used any diagram or visuals I have acknowledged the source in all instances,

4. this report has not and will not be submitted elsewhere for academic assessment in any other academic course.

Student data:

Name: Jonas Götte

Registration number: 6419097

Date: 31/07/2020

Signature: 

Appendix

Table 3: Data used for re-calibration. This data was retrieved from Savenije (1993) and the corrected intrusion length determined as described in Chapter 2.3.

Estuary	B_0 [m]	L [m]	Depth[m]	TidalAmp [m]	Q_f [m^3/s]	α	K	LHWS [km]	LHWS corrected [km]
Mae Klong	429	7592	4.29	1.438	60	7.2	0.3	25	26
Mae Klong	429	7592	4.29	1.438	36	6.2	0.3	35	36
Limpopo	392	8361	3.92	1.118	18	23.5	0.6	56	50
Limpopo	392	8361	3.92	1.118	32	16	0.6	43	37
Limpopo	392	8361	3.92	1.118	150	6.5	0.6	22	16
Limpopo	392	8361	3.92	1.118	10	30	0.6	64	58
Limpopo	392	8361	3.92	1.118	8	36	0.6	71	65
Tha Chin	239	9771	2.39	1.442	40	15	0.35	50	45
Tha Chin	239	9771	2.39	1.442	39	12	0.35	43	38
Incomati	199	10993	1.99	1.142	3	9.5	0.15	53	40
Incomati	199	10993	1.99	1.142	2	16	0.15	68	55
Incomati	199	10993	1.99	1.142	1	30	0.15	89	76
Pungue	450	10606	4.50	2.444	22	14	0.3	84	62
Pungue	450	10606	4.50	2.444	50	4.2	0.3	61	39
Pungue	450	10606	4.50	2.444	36	5.3	0.3	65	43
Pungue	450	10606	4.50	2.444	26	8	0.3	73	51
Pungue	450	10606	4.50	2.444	50	5	0.3	64	42
Thames	307	8853	3.07	2.322	40	6.3	0.2	101	69
Corantijn	996	28922	9.96	1.867	1995	0.4	0.21	50	17
Corantijn	996	28922	9.96	1.867	680	0.8	0.21	71	38
Corantijn	996	28922	9.96	1.867	115	1	0.21	84	51
Corantijn	996	28922	9.96	1.867	130	1.2	0.21	91	58
Corantijn	996	28922	9.96	1.867	220	1.1	0.21	88	55

Table 4: Estuary characteristics from Savenije (1993).

Estuaries	Country	B_0 (m)	h_0 (m)	a_1 (km)	$a_{(2)}$ (km)	x_1 (km)	$b_{(2)}$ (km)	H_0 (m)	K
1 Mae Klong	Thailand	250	5.2		102		155	2.2	0.30
2 Solo	Indonesia	220	9.2		226		226	0.8	0.60
3 Lalang	Indonesia	350	10.6		217		96	3.0	0.65
4 Limpopo	Mozambique	370	7.0		50		50	1.1	0.60
5 Tha Chin	Thailand	3600	5.3	22	87	22	87	2.6	0.35
6 ChaoPhya	Thailand	600	7.2		109		109	2.5	0.75
7 Incomati	Mozambique	4500	3.0	7	42	14	42	1.4	0.15
8 Pungue	Mozambique	6500	4.3		20		20	6.0	0.30
9 Maputo	Mozambique	9000	3.6	4	16	8	16	3.4	0.38
10 Thames	UK	7500	7.1		23		23	6.0	0.20
11 Eems	Netherlands	31600	3.9		19		19	3.6	0.30
12 Corantijn	Surinam	30000	6.5	19	64	18	48	2.3	0.21
13 Schelde	Netherlands	15200	10.0		26		28	3.7	0.25
14 Delaware	USA	37700	6.6		41		42	1.8	0.22
15 Tejo	Portugal	5820	7.0		11		11	3.4	0.90